Radiative neutrino mass generation linked to neutrino mixing and neutrinoless double beta decay predictions

Article (Submitted Version)

ULB-TH/14-04 USM-TH-320

Radiative neutrino mass generation linked to neutrino mixing and $0\nu\beta\beta$-decay predictions

Michael Gustafsson[a] **Jose M. No**[b] **and Maximiliano A. Rivera**[c]

[a] *Service de Physique Théorique, Université Libre de Bruxelles, B-1050 Bruxelles, Belgium*
[b] *Department of Physics and Astronomy, University of Sussex, BN1 9QH Brighton, UK*
[c] *Departamento de Física, Universidad Técnica Federico Santa María Casilla 110-V, Valparaiso, Chile*

mgustafs@ulb.ac.be, J.M.No@sussex.ac.uk, maximiliano.rivera@usm.cl

Abstract

We discuss the connection between the origin of neutrino masses and their mixings which arises in a class of scenarios with radiatively induced neutrino masses. In these scenarios, the neutrino mass matrix acquires textures with two entries close to zero in the basis where the charged-lepton mass matrix is diagonal. This results in specific constraints on the neutrino mixing parameters, which leads to the prediction of (i) a normal ordering of neutrino masses with the lightest neutrino mass in the $\sim$ meV range, and (ii) testable correlations among the various mixing angles, including a non-zero θ_{13} angle with its exact value correlated with the values of the atmospheric angle θ_{23} and the CP phase δ. We quantify the impact of deviations from exact zeroes in the mass matrix texture, and connect it to the amount of hierarchy among Yukawa couplings. These scenarios of radiative neutrino mass generation also give rise to new short-range contributions to neutrinoless double beta decay, which dominate over the usual light-neutrino exchange contribution. As a result, this class of models can have a sizable neutrinoless double beta decay rate, in the range of upcoming experiments despite the normal mass ordering of neutrinos.

1 Introduction

A central aspect of neutrino physics is the study of the origin and structure of the neutrino mass matrix, and its connection to the Dirac or Majorana nature of the neutrinos. Several appealing mechanisms have been advocated to account for the tiny but non-zero masses of neutrinos, ranging from the see-saw mechanism (see [1] for a review) to radiative neutrino mass generation (see *e.g.* [2–6]). The vast majority of these scenarios predict that neutrinos are of Majorana nature, but observationally it remains an open question. At the same time, the improved precision in the observed pattern of neutrino mixings has triggered a lot of theoretical activity aimed at explaining its origin based on ideas such as flavour symmetries (see [7] for a recent overview) or even anarchy [8].

It is not unconceivable that the same underlying new physics could be responsible for both the 10^{-2} – 10^{-1} eV neutrino mass scale and the observed pattern of neutrino masses and mixings, which would then provide a unified understanding of both aspects of neutrino physics. The purpose of this work is to explore a simple class of theories beyond the Standard Model (SM) in which this connection between the origin of neutrino masses and neutrino mixing naturally arises in the context of radiative neutrino mass generation. As we shall see, these scenarios also incorporate a rather unique link to the neutrinoless double beta ($0\nu\beta\beta$) decay probe of the Majorana nature of neutrinos.

As a starting point in our analysis, we consider how specific textures of the neutrino mass matrix m^ν can be responsible for the neutrino mass scale and mixing patterns. We focus on scenarios in which the neutrino mass matrix has one or several entries that are either exactly or approximate zero, so called "texture zeroes" [21–28]. Specifically, we look at cases with $m^\nu_{ee} \simeq 0$ and $m^\nu_{e\mu} \simeq 0$ (the precise definition of m^ν and an overview of its observational constraints from neutrino oscillation data will be presented in Section 2). Those scenarios incorporate nontrivial correlations among the various neutrino oscillation parameters, and can accommodate all the current observational data while giving interesting testable predictions for some of the unknowns in the neutrino sector. Of special interest are the predicted neutrino mass ordering and the correlation between the values of the reactor angle θ_{13}, the octant of the atmospheric angle θ_{23} and the CP phase δ.

It is then shown that such neutrino mass textures are obtained naturally in a class of models of radiative neutrino mass generation [31–34], thus providing an attractive embedding of neutrino mixings into a theory of neutrino mass generation. In this class of models, neutrino masses are generated at either 2- or 3-loop order, providing an elegant explanation for the smallness of neutrino masses compared to the electroweak scale [34,35] (some of these scenarios also incorporate an additional link to dark matter particle candidates [34]).

Finally, a generic feature of these scenarios is the existence of an important contribution to $0\nu\beta\beta$ decay from short-distance physics effects [31–33], resulting in potentially large amplitudes for $0\nu\beta\beta$ decay processes despite the fact that the standard contribution from light-neutrino exchange is extremely suppressed (since $m^\nu_{ee} \simeq 0$). This fact could make these processes detectable in ongoing and upcoming $0\nu\beta\beta$ decay experiments, including GERDA [37,38], EXO [39], SNO+ [40], KamLAND-Zen [41,42], CUORE [43], NEXT [44,45], MAJORANA [46] and SuperNEMO [47]. Remarkably, such scenarios give a detectable signal in $0\nu\beta\beta$ decay experiments together with a normal ordering of the neutrino masses.

The paper is organized as follows: In section 2, we introduce our conventions for the neutrino mass matrix and review the present experimental situation for neutrino masses and mixings from neutrino oscillations. In section 3, the correlations among different neutrino parameters are studied in detail for scenarios in which $m^\nu_{ee} = 0$, and special attention is put on the scenario $m^\nu_{ee} = m^\nu_{e\mu} = 0$ which will be central in the rest of the paper. In section 4 we identify and explore a class of radiative neutrino mass generation scenarios that naturally generate a neutrino mass matrix with approximate texture zeroes of the same form as those studied in section 3. We then define a technical measure of the amount of hierarchy (in the neutrino "Yukawa" matrix) for these scenarios and show that it is indeed milder than in the charged-lepton sector. In section 5 we explore the features of the leading, short-distance contribution to $0\nu\beta\beta$ decay in these scenarios and derive prospects of detection in various present and future $0\nu\beta\beta$ decay experiments. Finally, we conclude in section 6.

2 Conventions and neutrino oscillation data

For the case of Majorana neutrinos, a parametrization of their mass matrix, in the basis where charged current interactions are flavour-diagonal and the charged leptons e, μ, τ are simultaneously mass eigenstates, reads

$$m^\nu = U^T\, m^\nu_D\, U \quad \text{with} \quad m^\nu_D = \text{Diag}\,(m_1, m_2, m_3)\,. \tag{2.1}$$

Here $m_{1,2,3}$ are the masses of the three light neutrinos and U^T is the PMNS matrix [9], given in terms of three mixing angles θ_{12}, θ_{23}, θ_{13} and three phases (a CP phase δ and two Majorana phases[1] α_1 and α_2),

$$U = \text{Diag}\left(1, e^{i\alpha_1}, e^{i(\alpha_2+\delta)}\right) \times \begin{pmatrix} c_{13}c_{12} & -c_{23}s_{12} - s_{23}c_{12}s_{13}e^{i\delta} & s_{23}s_{12} - c_{23}c_{12}s_{13}e^{i\delta} \\ c_{13}s_{12} & c_{23}c_{12} - s_{23}s_{12}s_{13}e^{i\delta} & -s_{23}c_{12} - c_{23}s_{12}s_{13}e^{i\delta} \\ s_{13}e^{-i\delta} & s_{23}c_{13} & c_{23}c_{13} \end{pmatrix}, \tag{2.2}$$

with $s_{ij} \equiv \sin(\theta_{ij})$ and $c_{ij} \equiv \cos(\theta_{ij})$. Investigating the presence (or absence) of an organizing principle behind the observed structure in m^ν_D and the PMNS matrix U is then a central aspect of neutrino phenomenology. This in turn requires an accurate experimental determination of the various neutrino parameters, in particular the neutrino mass ordering, the three mixing angles and the CP phase.

Until the year 2011, there existed only an experimental upper bound on the value of the mixing angle θ_{13}, while θ_{23} and θ_{12} were relatively well determined and consistent with the tri-bi-maximal [10] neutrino mixing hypothesis $\theta_{12} = 30^\circ$, $\theta_{23} = 45^\circ$, $\theta_{13} = 0^\circ$. However, the recent experimental data from Daya-Bay [11], RENO [12], Double Chooz [13], T2K [14] and MINOS [15], measuring a nonzero value for θ_{13}, combined with the latest results from atmospheric neutrinos [16, 17] which are possibly suggesting a departure of the atmospheric angle θ_{23} from its maximal mixing value $\pi/4$, have provided us with a new perspective on neutrino mixing. This is summarized in the up-to-date global fits to neutrino oscillation data in [18–20]. Of them, we shall use [20], which gives $\Delta m^2_{21} \equiv m_2^2 - m_1^2 = 7.50^{+0.18}_{-0.19} \times 10^{-5}\text{eV}^2$,

[1] We adopt here the convention for the Majorana phases given in [23].

$|\Delta m^2_{31}| \equiv |m^2_3 - m^2_1| = 2.473^{+0.07}_{-0.067} \times 10^{-3}\text{eV}^2$ ($2.427^{+0.065}_{-0.042} \times 10^{-3}\text{eV}^2$) for $\Delta m^2_{31} > 0$ ($\Delta m^2_{31} < 0$), $s^2_{12} = 0.302^{+0.013}_{-0.012}$, $s^2_{13} = 0.0227^{+0.0023}_{-0.0024}$ and $s^2_{23} = 0.413^{+0.037}_{-0.025}$ ($0.594^{+0.021}_{-0.022}$) if on the first (second) octant for θ_{23}.

Neutrino oscillation experiments are still not sensitive to the sign of Δm^2_{31} which results in two possible mass orderings in the neutrino sector, commonly known as Normal Ordering (NO) and Inverted Ordering (IO), that are characterized by:

$$\begin{array}{lcll} \Delta m^2_{31} > 0 & \rightarrow & m_1 < m_2 < m_3 & (\text{NO}) \\ \Delta m^2_{31} < 0 & \rightarrow & m_3 < m_1 < m_2 & (\text{IO})\,. \end{array} \tag{2.3}$$

Also, while non-maximal θ_{23} mixing seems now favored, current experimental data are not sensitive to the sign of its deviation from maximality (see [18, 20] for a discussion on this issue). Finally, the value of the CP phase δ is also beyond current experimental sensitivity, although it is expected that future measurements from T2K and NOνA will begin to constrain the CP phase.

3 Zeroes of the neutrino mass matrix

We now motivate and discuss scenarios in which some of the entries of the neutrino mass matrix (2.1) are exactly or approximately zero. We will analyze mass textures for m^ν_{ab} with $m^\nu_{ee} \simeq 0$. There are only three such textures allowed by neutrino oscillation data [21]:

$$\begin{pmatrix} 0 & \times & \times \\ \times & \times & \times \\ \times & \times & \times \end{pmatrix}, \qquad \begin{pmatrix} 0 & 0 & \times \\ 0 & \times & \times \\ \times & \times & \times \end{pmatrix}, \qquad \begin{pmatrix} 0 & \times & 0 \\ \times & \times & \times \\ 0 & \times & \times \end{pmatrix}, \tag{3.4}$$

where the $\times$ denote non-vanishing (not necessarily equal) entries. In this section we focus on the case of exact texture zeroes, and leave the discussion of approximate zeroes and its connection to radiative generation of neutrino masses for section 4.

The (complex) neutrino mass matrix is, for the case of Majorana neutrinos, a function of nine independent parameters, of which six are measurable via neutrino oscillations[2]. Setting any matrix element to zero then gives two equations (both its real and imaginary part have to vanish) which impose correlations among various neutrino parameters. From Eq. (2.2), the textures in (3.4) give the following relations:

$$m^\nu_{ee} \equiv c^2_{13}\left(m_1 c^2_{12} + e^{2i\alpha_1} m_2 s^2_{12}\right) + e^{2i\alpha_2} m_3 s^2_{13} = 0\,, \tag{3.5}$$

$$m^\nu_{e\mu} \equiv c_{13}\left[\left(e^{2i\alpha_1} m_2 - m_1\right) s_{12} c_{12} c_{23} + e^{i\delta} s_{23} s_{13}\left(e^{2i\alpha_2} m_3 - m_1 c^2_{12} - e^{2i\alpha_1} m_2 s^2_{12}\right)\right] = 0\,, \tag{3.6}$$

$$m^\nu_{e\tau} \equiv c_{13}\left[\left(m_1 - e^{2i\alpha_1} m_2\right) s_{12} c_{12} s_{23} + e^{i\delta} c_{23} s_{13}\left(e^{2i\alpha_2} m_3 - m_1 c^2_{12} - e^{2i\alpha_1} m_2 s^2_{12}\right)\right] = 0\,. \tag{3.7}$$

An immediate question that arises is if the above textures give a prediction for the neutrino mass ordering. From the condition (3.5), which is common to all three textures,

[2]Neutrino oscillations are not sensitive to the Majorana phases α_1 and α_2 nor to the absolute neutrino mass scale.

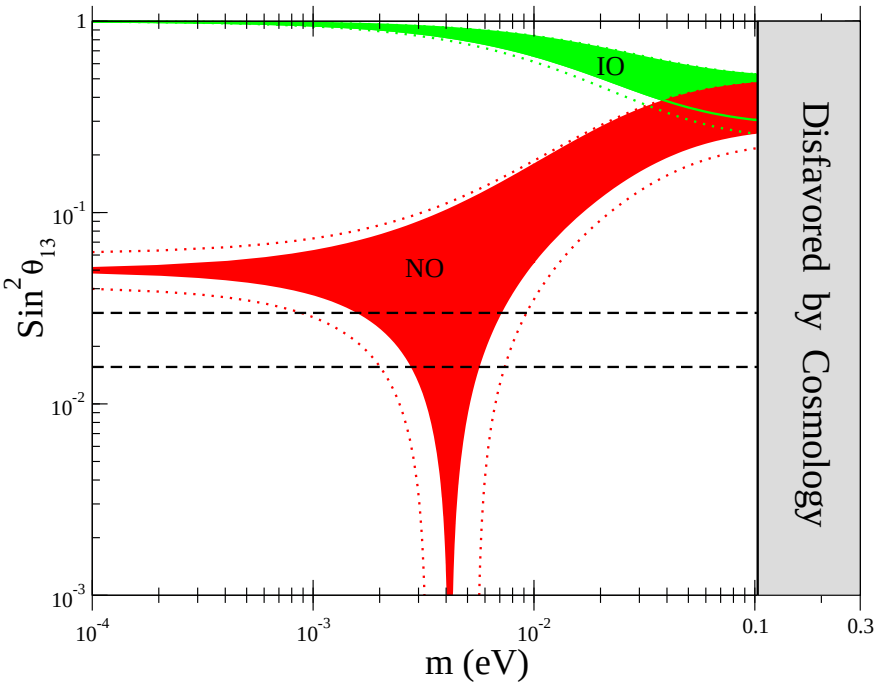

Figure 1: Allowed regions for θ_{13} as a function of the lightest neutrino mass m for a neutrino mass matrix with texture $m^{\nu}_{ee} = 0$. The regions are for normal (NO/red) and inverted (IO/green) mass ordering, with best-fit measured values of θ_{12}, Δm^2_{13} and Δm^2_{21} (solid region) as given in [20]. The allowed region with θ_{12}, Δm^2_{13} and Δm^2_{21} within their 3σ experimental ranges (dotted line) is also shown. The dashed-black horizontal lines enclose the 3σ allowed experimental range for θ_{13}. The grey region is disfavored by cosmological data [30].

we already obtain information on possible ranges of neutrino masses and mixing angles. In particular, from Eq. (3.5) it follows that θ_{13} is constrained to

$$\frac{|s^2_{12}\, m_2 - c^2_{12}\, m_1|}{m_3} \leq t^2_{13} \leq \frac{s^2_{12}\, m_2 + c^2_{12}\, m_1}{m_3} \tag{3.8}$$

with $t_{13} \equiv \tan(\theta_{13})$. This allows us to obtain in a straightforward manner the allowed range of solutions for normal (NO) and inverted (IO) ordering in the (m, θ_{13}) plane, where m is the mass of the lightest neutrino:

- NO: $m_1 = m$, $m_2 = \sqrt{\Delta m^2_{21} + m^2}$, and $m_3 = \sqrt{\Delta m^2_{31} + m^2}$.
- IO: $m_1 = \sqrt{|\Delta m^2_{31}| + m^2}$, $m_2 = \sqrt{|\Delta m^2_{31}| + \Delta m^2_{21} + m^2}$, and $m_3 = m$.

The range of solutions to Eq. (3.8) for NO and IO are shown in Figure 1, both for θ_{12}, Δm^2_{31} and Δm^2_{21} set to their best-fit values (solid regions) and with these parameters allowed to vary independently within their 3σ experimental ranges (inside dotted lines). As can be seen from Figure 1, the experimental constraint on the reactor mixing angle θ_{13} excludes the inverted mass ordering scenario when $m^{\nu}_{ee} = 0$, and thus all the three textures in (3.4) predict a normal ordering for the neutrino masses. From Figure 1 it is also clear that Eq. (3.5) is only satisfied in a limited range of values for m as a function of θ_{13} [23, 29] (this range is

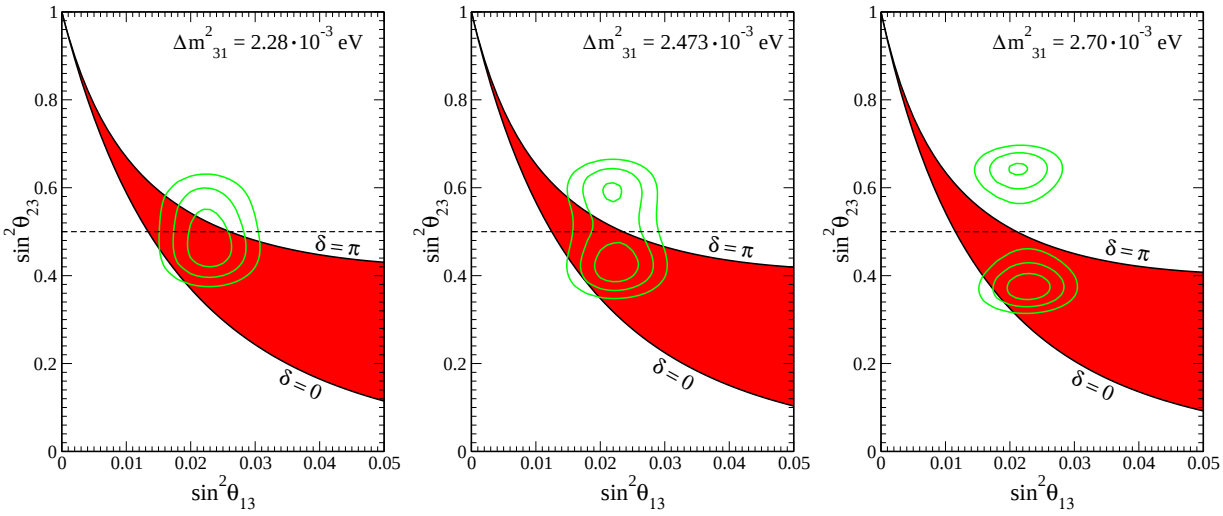

Figure 2: Allowed regions for the neutrino mass texture $m^\nu_{ee} = m^\nu_{e\mu} = 0$ in the $(s^2_{13},\ s^2_{23})$ plane (solid-red), for Δm^2_{31} fixed at its -3σ value (LEFT), best-fit value (MIDDLE) and $+3\sigma$ value (RIGHT), and best-fit values of Δm^2_{21} and s^2_{12}. In each case, the 1σ, 2σ and 3σ allowed experimental contours from the global analysis of [20] are shown in green. The horizontal dashed line indicates maximal mixing $\theta_{23} = \pi/4$.

commonly referred to as "the chimney"). For the oscillation parameters within their 3σ allowed experimental range, m must lie in the interval 0.001 eV $\lesssim m \lesssim$ 0.009 eV.

As can be seen from Eq. (3.5), m^ν_{ee} does not depend on the atmospheric mixing angle θ_{23} or the CP phase δ. We will now analyze how an extra zero in the texture leads to further relations among the various neutrino oscillation parameters, which also involve θ_{23} and δ.

3.1 Mass texture with $m^\nu_{ee} = 0$ and $m^\nu_{e\mu} = 0$

For the case of two independent texture zeroes in m^ν, such as Eqs. (3.5) and (3.6), these form a system of four equations (vanishing real and imaginary parts of m^ν_{ee} and $m^\nu_{e\mu}$). This system of equations links the values of δ, α_1, α_2 and m to the values of the neutrino oscillation parameters Δm^2_{21}, Δm^2_{31}, θ_{12}, θ_{23} and θ_{13}, and leads to specific predictions of m, δ, α_1 and α_2 (up to an overall sign change in δ, α_1 and α_2) when the other parameters are specified. Moreover, solutions will only exist for certain values of Δm^2_{21}, Δm^2_{31}, θ_{12}, θ_{23} and θ_{13}, so the imposition of such textures result in non-trivial relations among these parameters.[3]

As is clear from the discussion in the previous section, the requirement $m^\nu_{ee} = 0$ resulted in specific relations among θ_{12}, θ_{13} and the lightest neutrino mass m. Requiring also $m^\nu_{e\mu} = 0$ does not alter these correlations. However, whereas $m^\nu_{ee} = 0$ imposed no constraints on the possible values of the atmospheric mixing angle θ_{23} and the CP phase δ, the further requirement of $m^\nu_{e\mu} = 0$ gives rise to additional links between the values of these two and the other neutrino oscillation parameters. In particular it correlates the allowed values of θ_{13}, θ_{23} and δ, as shown in Figures 2 and 3.

[3]Neutrino mass matrix textures with more than two entries set to zero would over-constrain the system, and has no solution for m_1, δ, α_1 and α_2 given the current neutrino oscillation data [21].

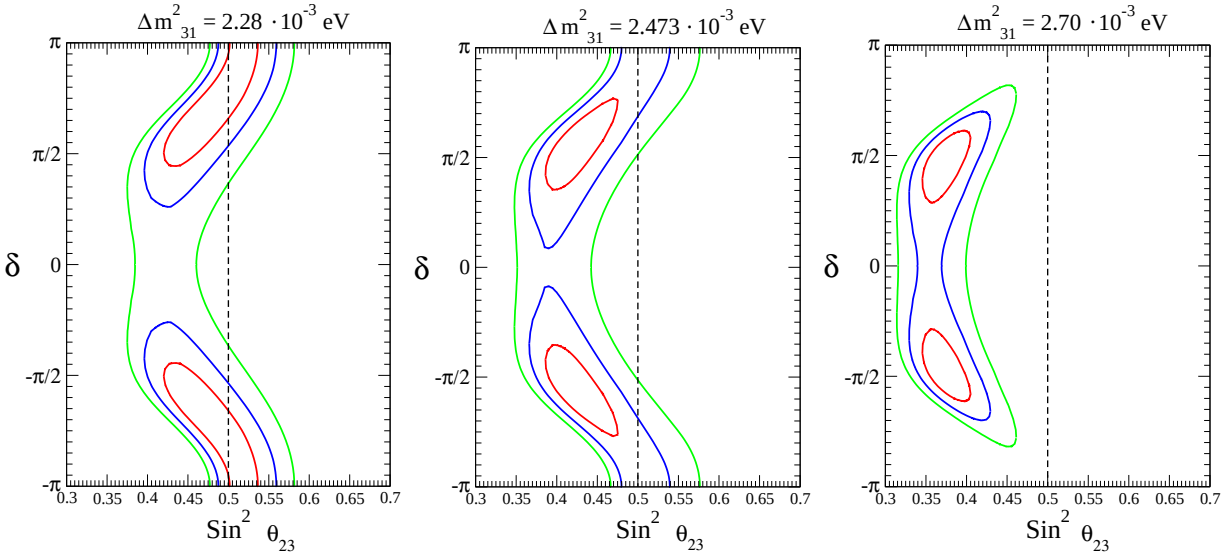

Figure 3: Allowed values of the CP phase δ (for the neutrino mass texture $m^\nu_{ee} = m^\nu_{e\mu} = 0$) as a function of s^2_{23} along the 1σ (red), 2σ (blue) and 3σ (green) experimental contours from Figure 2. The values of Δm^2_{31}, Δm^2_{21} and s^2_{12} are set as in Figure 2. The vertical dashed line indicates maximal mixing $\theta_{23} = \pi/4$.

From Eqs. (3.5) and (3.6) it is possible to derive a "master formula" correlating all the neutrino oscillation parameters (see Appendix I for details). For a normal ordering (NO)

$$\frac{\Delta m^2_{21}}{\Delta m^2_{31}} = s^2_{13}\,\frac{t^2_{23}}{t^2_{12}}\,\frac{1 - t^4_{12} + 2 s_{13}\,t^2_{12}\,t^{-1}_{23}\left(t^{-1}_{12} + t_{12}\right)\cos\delta}{c^4_{13} - s^2_{13}\left(t^2_{12}\,t^2_{23} - 2 s_{13}\,t_{12}\,t_{23}\cos\delta + s^2_{13}\right)}\,. \tag{3.9}$$

It is important to stress that this relation might not have been compatible with current neutrino oscillation experimental data. However, it happens to fit the data well (see *e.g.* Appendix I), and furthermore it gives clear predictions for the correlations among future precision data in the neutrino sector. For small values of θ_{13}, the right-hand side of Eq. (3.9) can be expanded in powers of s_{13}, which to lowest orders then reads

$$\frac{\Delta m^2_{21}}{\Delta m^2_{31}} = s^2_{13}\,\frac{t^2_{23}}{t^2_{12}}\left[\left(1 - t^4_{12}\right) + 2\,s_{13}\,\frac{t_{12}\,\left(1 + t^2_{12}\right)}{t_{23}}\,\cos\delta\right] + \mathcal{O}(s^4_{13})\,. \tag{3.10}$$

In Figure 2 we show the allowed region (solid-red) from Eq. (3.9) in the (s^2_{13}, s^2_{23}) plane for Δm^2_{31} fixed at its best-fit value (MIDDLE) and at its -/+3σ value (LEFT/RIGHT). Both Δm^2_{21} and s^2_{12} are fixed to their best-fit values in Figure 2 (but a marginalization over these parameters would also give almost identical experimental contour regions). The upper bound on s^2_{23} as a function of s^2_{13} corresponds to $\delta = \pm\pi$, and the lower bound corresponds to $\delta = 0$, which can be understood from Eq. (3.10). Also shown are the 1σ, 2σ and 3σ experimentally allowed regions (green lines) from the global analysis of [20, 71].

As can be seen from Figure 2, the allowed range of the atmospheric mixing angle θ_{23} for a neutrino mass texture with $m^\nu_{ee} = m^\nu_{e\mu} = 0$ is not symmetric around $\theta_{23} = \pi/4$ ($s^2_{23} = 1/2$), and a value of $\theta_{23} < \pi/4$ seems favored given current experimental constraints on the value of θ_{13}. This preference for the lower θ_{23}-octant is only very mild for $\Delta m^2_{31} = 2.28 \cdot 10^{-3}$ eV

(and in fact, in this case it is not very well motivated to talk about the θ_{23}-octant, since the preferred region for θ_{23} lies close to $\pi/4$), and becomes more pronounced for increasing Δm^2_{31}. The conclusion of a preferred $\theta_{23} < \pi/4$ depends also weakly on the precise value of the solar angle θ_{12}, since for values of θ_{12} significantly larger than the best-fit value the red region in Figure 2 is shifted upwards and eventually covers a sizable part of the upper octant as well. Thus, a future, more accurate determination of the value of θ_{12} could either reinforce this conclusions or make the preference for the lower θ_{23}-octant in this texture eventually disappear.

The mass texture with $m^\nu_{ee} = m^\nu_{e\mu} = 0$ also results in interesting correlations among the values of θ_{13}, θ_{23} and the CP phase δ, as shown in Figure 3. Here the 1σ, 2σ and 3σ allowed experimental regions of s^2_{13} *vs* s^2_{23} are plotted in the (δ, s^2_{23}) plane for the same values of Δm^2_{31}, Δm^2_{21}, s^2_{12} as adopted in the three plots in Figure 2 (Note that since for $m^\nu_{ee} = m^\nu_{e\mu} = 0$ there are only two independent parameters out of the three parameters θ_{13}, θ_{23}, δ, we can always extract the prediction of δ along any contour in the (s^2_{13}, s^2_{23}) plane). We see that values of $|\delta| \sim \pi/2$ become more favored for increasing Δm^2_{31}, while for $\Delta m^2_{31} \sim 2.28 \cdot 10^{-3}$ eV values $|\delta| > \pi/2$, and in particular $|\delta| \to \pi$, are preferred. Figure 3 also shows a specific correlation between the values of θ_{23} and δ within this texture: larger values of θ_{23} seem to favor larger values of $|\delta|$. Finally, it is important to notice that the texture does not impose any restriction on the sign of the CP phase, since δ appears in Eq. (3.9) as $\cos\delta$.

3.2 Mass texture with $m^\nu_{ee} = 0$ and $m^\nu_{e\tau} = 0$.

The entry $m^\nu_{e\tau}$ of the neutrino mass matrix is similar in structure to $m^\nu_{e\mu}$, and can in fact be obtained from the latter via the substitutions $\theta_{23} \to \pi/2 - \theta_{23}$ and $\delta \to \delta + \pi$. Then the correlation between θ_{13} and θ_{23} for $m^\nu_{ee} = m^\nu_{e\tau} = 0$ is opposite to the one found for $m^\nu_{ee} = m^\nu_{e\mu} = 0$ in the previous section, since now $s^2_{23} \to c^2_{23}$. In particular, for $m^\nu_{ee} = m^\nu_{e\tau} = 0$, $\theta_{23} > \pi/4$ (second octant) is now favored. Furthermore, both entries $m^\nu_{e\tau}$ and $m^\nu_{e\mu}$ cannot vanish at the same time. For $m^\nu_{ee} = 0$ it can be shown that

$$\left|m^\nu_{e\mu}\right|^2 + |m^\nu_{e\tau}|^2 = c^2_{13}\left[(s_{12}\, c_{12})^2\left(\sqrt{\Delta m^2_{21} + m^2} - m\right)^2 + s^2_{13}\left(1 + t^2_{13}\right)^2\left(\Delta m^2_{31} + m^2\right)\right]. \qquad (3.11)$$

For Δm^2_{21}, Δm^2_{31}, s^2_{12} and s^2_{13} inside their 3σ allowed experimental ranges, we find the following bound $\sqrt{\left|m^\nu_{e\mu}\right|^2 + |m^\nu_{e\tau}|^2} \geq 0.0063$ eV, where the inequality is saturated for $m \lesssim 0.009$ eV. Therefore, a texture with $m^\nu_{ee} = m^\nu_{e\mu} = m^\nu_{e\tau} = 0$, is not possible.

It is worth stressing that if $m^\nu_{ee} = 0$ and either of $m^\nu_{e\mu} = 0$ or $m^\nu_{e\tau} = 0$ are imposed, the allowed ranges for the rest of the neutrino mass matrix entries are very constrained (once the current neutrino oscillation allowed experimental ranges are also imposed). This can be explicitly seen in Figure 4 for the case $m^\nu_{ee} = m^\nu_{e\mu} = 0$, where the allowed ranges of the neutrino mass matrix entries $|m^\nu_{e\tau}|$, $\left|m^\nu_{\mu\mu}\right|$, $\left|m^\nu_{\mu\tau}\right|$ and $|m^\nu_{\tau\tau}|$ is computed from a scan over all experimentally allowed values of the neutrino oscillation parameters Δm^2_{21}, Δm^2_{31}, s^2_{12}, s^2_{23} and s^2_{13}. In order to perform the scan, random initial condition are given to the unconstrained parameters δ, α_1, α_2 and m (< 0.1 eV) and we generate $\gtrsim 10^6$ numerical solutions to

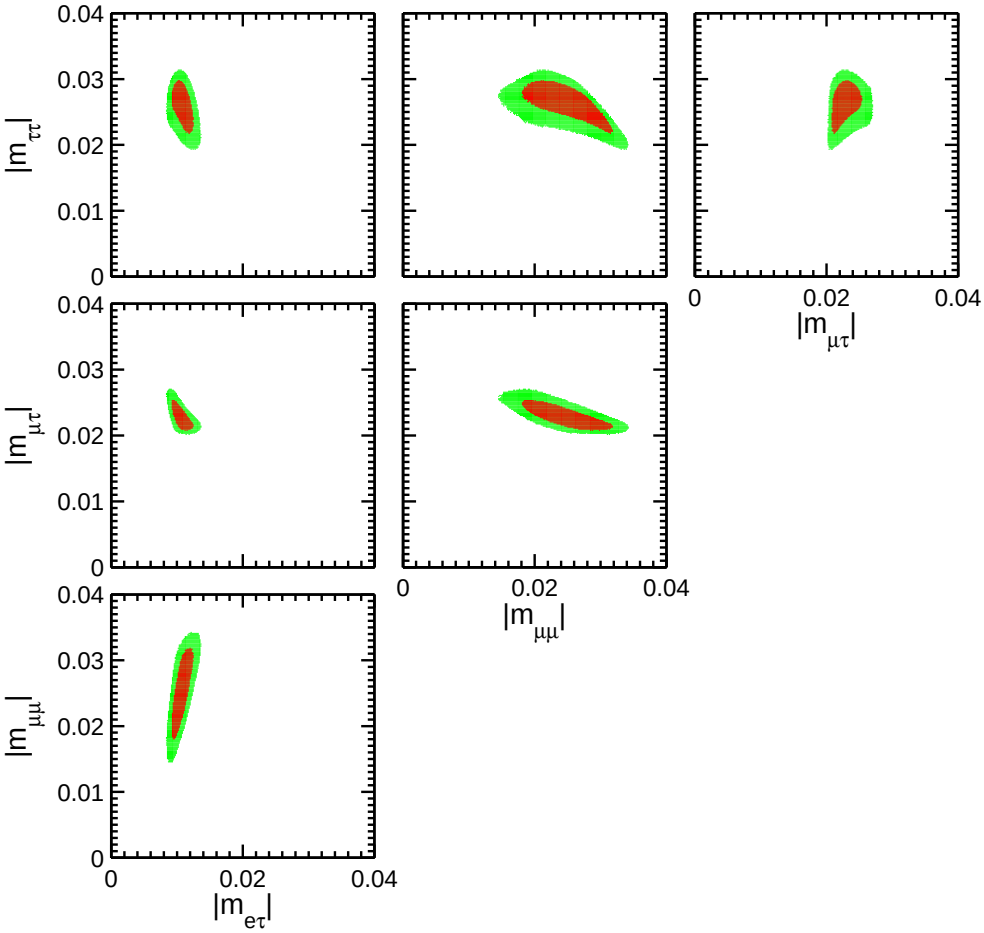

Figure 4: The size of the entries in the neutrino mass matrix $|m^\nu_{e\tau}|$, $|m^\nu_{\mu\mu}|$, $|m^\nu_{\mu\tau}|$ and $|m^\nu_{\tau\tau}|$ (in eV) for mass textures with $m^\nu_{ee} = m^\nu_{e\mu} = 0$. The red regions correspond to the allowed values for neutrino oscillation data within 1σ confidence level, while the green regions correspond to the allowed values for neutrino oscillation data within 3σ confidence level.

$m^\nu_{ee} = m^\nu_{e\mu} = 0$. The 1σ and 3σ allowed regions for the neutrino mass matrix entries $|m^\nu_{ab}|$ are found from those random-scan points by calculating each scan-point's total log-likelihood relative to the best-fit value $\Delta \ln \mathcal{L}$ and finding the points with $-2\Delta \ln \mathcal{L} < 5.88$ and 18.2, respectively. These limiting values on $2\Delta \ln \mathcal{L}$ are the appropriate values for five degrees of freedom, corresponding to the five measured neutrino-oscillation parameters. Technically speaking, the total likelihood function $\mathcal{L}$ is built-up from the product of uncorrelated single Gaussian probability distribution functions (pdfs) for each observable, except for the θ_{23} pdf which is instead modelled as the sum of two properly normalised Gaussian pdfs with minima in two separate octants and a third Gaussian pdf around the maximal mixing value $\pi/4$, all in order to properly match the result presented in [71].[4]

[4]We use their "Huber Fluxes, no RSBL" v1.2 results.

4 Textures from radiative neutrino mass generation

We now discuss the connection between the neutrino mass textures analyzed in the previous section and scenarios of neutrino mass generation. In particular, we will show that a certain type of scenario for radiative neutrino mass generation naturally leads to approximate mass textures of the form (3.4).

Let us begin by simply noting that beyond SM (BSM) physics must be Lepton Number Violating (LNV) in order to allow for the generation of Majorana masses for the light neutrinos. Then, by assuming that no extra gauge symmetries beyond the electroweak $SU(2)_L \times U(1)_Y$ are present, we can parametrize the effect of the LNV new physics in terms of non-renormalizable operators that include only SM fields and preserve all the local symmetries of the SM. We assume that the LNV physics couples only directly to leptons, but not directly to quarks. Under these generic assumptions, it has recently been shown in [33] that when the LNV physics couples only directly to leptons of right-handed chirality ℓ_R (and not to those of left-handed chirality), then the only lowest-order operator (appearing at dimension $D = 9$) that violates Lepton Number by two units ($\Delta L = 2$) is given by[5]

$$\mathcal{O}^9 \equiv C^{(9)}_{ab}\, \overline{\ell^c}_{R_a} \ell_{R_b} \left[(D_\mu H)^T\, i\sigma_2 H \right]^2 \tag{4.12}$$

with $C^{(9)}_{ab}$ being a matrix in flavor space. This is part of a more general result in [33] regarding the dimensions and structure of the lowest-order LNV non-renormalizable SM operators involving leptons and no quarks[6]. Upon electroweak symmetry breaking, $\mathcal{O}^9$ induces a term

$$\frac{C^{(9)}_{ab}}{\tilde{\Lambda}}\, \overline{\ell^c}_{R_a} \ell_{R_b} W^+_\mu W^{+\mu}. \tag{4.13}$$

We stress that the scale $\tilde{\Lambda}$ may not directly correspond to any specific new physics scale, but rather to a combination of different mass scales, and in particular it might be lower than any of those in scenarios with some hierarchy of scales. The term (4.13) generates a leading contribution to neutrino masses at 2-loops, with two chirality flips, as shown in Figure 5. Implications of $\mathcal{O}^9$ for $0\nu\beta\beta$ decay will be analyzed in section 5. The neutrino mass matrix m^ν_{ab} in this scenario is then proportional to the charged-lepton masses $m_{l_a}\, m_{l_b}$ (since weak charged currents conserve lepton flavor):

$$m^\nu_{ab} \sim \left(\frac{1}{16\,\pi^2} \right)^n C^{(9)}_{ab}\, \frac{m_{l_a}\, m_{l_b}}{\Lambda}\,, \tag{4.14}$$

where Λ can be related to $\tilde{\Lambda}$. Both the loop suppression and $C^{(9)}_{ab}/\Lambda$ will ultimately depend[7] on the specific LNV new physics responsible for neutrino mass generation.

[5] Note that this operator does not appear in the classification of SM $\Delta L = 2$ effective operators in [48,49], as LNV effective operators involving SM gauge bosons were in [48] thought to be unable to accommodate a suitable renormalizable completion – see also [50] for a brief discussion on this issue.

[6] The lowest-order operator involving only leptons of right-handed chirality appears at $D = 9$, while the lowest-order operator involving both left and right-handed chiralities appears at $D = 7$. The lowest-order operator involving only left-handed leptons is the well-known D=5 *Weinberg operator* [36].

[7] While neutrino masses generated from $\mathcal{O}^9$ in (4.12) appear at 2-loops, the operator $\mathcal{O}^9$ may itself have been generated at loop order in an underlying renormalizable completion (see Section 4.2), and thus $n \geq 2$.

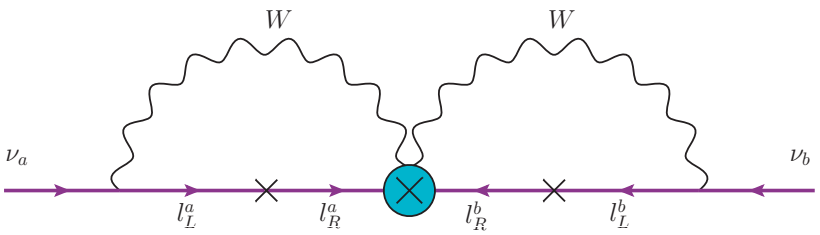

Figure 5: The 2-loop diagram generating neutrino masses from $\mathcal{O}^9$ in Eq. (4.12). The crosses $\times$ in the fermion propagators represent chirality flips, which (upon electroweak symmetry breaking) make this Feynman amplitude proportional to the masses m_{l_a} and m_{l_b}.

It is apparent from Eq. (4.14) that due to the $m_{l_a}\, m_{l_b}$ dependence, the entries in the neutrino mass matrix m^ν_{ab} proportional to m_{l_e} will be expected to be much smaller than the rest (up to the size of $C^{(9)}_{ab}$, see discussion below), since $m_{l_\tau} \gg m_{l_\mu} \gg m_{l_e}$. This suppression of certain mass matrix elements leads *naturally* to a matrix texture including approximate zeroes. These zeroes will not be exact unless the corresponding $C^{(9)}_{ab} = 0$. Nevertheless, the predictions for the neutrino mass ordering (NO *vs* IO), absolute neutrino mass scale m, octant of θ_{23} and CP phase δ presented in Section 3 are still exactly verified for small enough entries. Figure 6 (LEFT and RIGHT) shows that this occurs for $|m^\nu_{ee}|\,, \left|m^\nu_{e\mu}\right| \lesssim 10^{-4}$ eV. However, as the size of the entries m^ν_{ee}, $m^\nu_{e\mu}$ increases, there is a transition region in which these predictions get fainter, eventually disappearing for $|m^\nu_{ee}|\,, \left|m^\nu_{e\mu}\right| \gtrsim 10^{-3}$ eV.

The appearance of these approximate texture zeroes therefore depends on the value of $C^{(9)}_{ee}/\Lambda$, since at least $|m^\nu_{ee}| \lesssim 10^{-4}$ eV is needed to generate the same predictions as for the exact zeroes (see Figure 6 LEFT). Given this fact, Eq. (4.14) predicts the textures (3.4) above a certain effective scale Λ_L (with $C^{(9)}_{ee}/\Lambda \sim \Lambda_L^{-1}$), approximately given by $\Lambda_L \gtrsim 100$ GeV (for $n = 2$), $\Lambda_L \gtrsim 600$ MeV (for $n = 3$) and $\Lambda_L \gtrsim 4$ MeV (for $n = 4$).

The existence of renormalizable completions of $\mathcal{O}^9$ giving rise to the relation (4.14) with an effective scale lower than Λ_L cannot be fully discarded (recall that Λ does not directly correspond to the scale of any new physics in the sense of an effective field theory), as it depends ultimately on the details of the BSM LNV sector. However, since the LNV new physics must involve states with non-zero hypercharge and sizable couplings to leptons, scenarios with effective scales $\lesssim \Lambda_L$ seem difficult to obtain (specially for $n \geq 3$) without being already in conflict with high energy collider data.

On the other hand, $C^{(9)}_{ab}/\Lambda$ cannot be arbitrarily small if one is to be compatible with neutrino oscillation data. This is due to the fact that for $|m^\nu_{ee}|\,, \left|m^\nu_{e\mu}\right| \ll \sqrt{\Delta m^2_{21}}$ the rest of the entries m^ν_{ab} cannot be very small if one is to be compatible with experimental neutrino oscillation data (recall Figure 4), and in particular $|m^\nu_{e\tau}| \gtrsim 0.008$ eV. From this requirement, an approximate upper bound Λ_H (with $C^{(9)}_{e\tau}/\Lambda \sim \Lambda_H^{-1}$) can be obtained. We find $\Lambda_H \lesssim 5$ TeV, $\Lambda_H \lesssim 30$ GeV and $\Lambda_H \lesssim 200$ MeV for $n = 2$, $n = 3$ and $n = 4$, respectively. We will from now on restrict ourselves to the cases $n = 2$ and $n = 3$, since again scenarios with effective scales $\lesssim \Lambda_H$ seem difficult to obtain for $n \geq 4$.

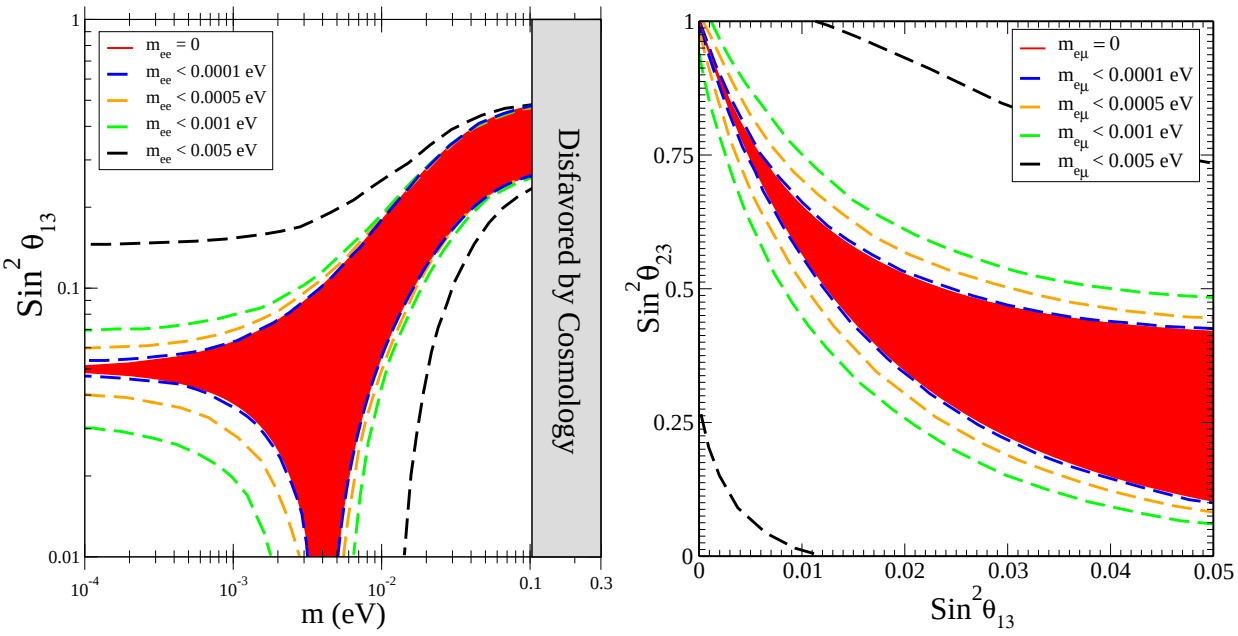

Figure 6: LEFT: For normal ordering (NO), allowed region in the (m, s^2_{13}) plane as the upper bound on $|m^\nu_{ee}|$ is increased. RIGHT: For $m^\nu_{ee} = 0$, allowed region in the (s^2_{13}, s^2_{23}) plane as the upper bound on $\left|m^\nu_{e\mu}\right|$ is increased. In both cases, we consider the best-fit values for the other neutrino oscillation parameters [20].

4.1 Approximate textures and a measure of hierarchy

If all the entries in the "Yukawa" matrix $C^{(9)}_{ab}$ are of the same order, the size of the entries in the neutrino mass matrix m^ν_{ab} in Eq. (4.14) will all be very hierarchical. This is clearly disfavored by neutrino oscillation data, which allow for at most two independent texture zeroes [21] and require that the remaining entries in m^ν_{ab} are all of a size between $\sqrt{\Delta m^2_{21}}$ and $\sqrt{\Delta m^2_{31}}$ (see Figure 4). Then, in order to be compatible with oscillation data a certain degree of hierarchy among the different entries $C^{(9)}_{ab}$ will be needed. This degree of hierarchy in a specific "Yukawa" matrix $C^{(9)}_{ab}$ can be quantified by means of Eq. (4.14) and using the neutrino oscillation data as input for m^ν_{ab}. We choose to define the hierarchy of $C^{(9)}_{ab}$ in the charged-lepton mass eigenstate basis. We look at the hierarchy among the absolute values of the neutrino mass matrix entrances (note however that they are in general complex entries with their relative phase adjusted to agree with experimental data).[8] The degree of hierarchy Π is then defined as

$$\Pi^2 = \min_N \sum_{a \geq b} \left[\log \left(N \frac{|m^\nu_{ab}|}{m_{l_a} m_{l_b}} \right) \right]^2 . \tag{4.15}$$

The constant N is introduced, and minimized over, in order to account for the fact that the definition of hierarchy should not be dependent on the overall $C^{(9)}_{ab}$ normalization. Π in

[8] Alternatively, we could have defined the hierarchy by means of the eigenvalues of $C^{(9)}_{ab}$, which yields different but qualitatively similar results. However, in that case the connection between $C^{(9)}_{ab}$, neutrino oscillation parameters and charged-lepton masses is not apparent.

(4.15) then provides us with a way to quantify the minimal amount of hierarchy required in $C_{ab}^{(9)}$ and still be compatible with data from neutrino oscillation experiments. In Figure 7 we show point with the minimal amount of hierarchy Π and the corresponding values of $|m_{ee}^{\nu}|$ as a function of m, when the neutrino oscillation parameters θ_{12}, θ_{23}, θ_{13}, Δm_{13}^2 and Δm_{21}^2 are set to their best-fit values. These points have been obtained numerically using a global minimization[9] in the neutrino parameters δ, α_1 and α_2, as well as in N. As seen in Figure 7, the region with the lowest hierarchy corresponds to $|m_{ee}^{\nu}| \sim 10^{-7}$ eV, and altogether the region of very small $|m_{ee}^{\nu}|$ ("the chimney") has a substantially lower hierarchy than the rest of the regions in the (m, $|m_{ee}^{\nu}|$) plane. The lowest hierarchy ($\Pi \sim 5.5$) is obtained for $m \sim 0.0045$ eV and $|m_{ee}^{\nu}| \sim 10^{-7}$ eV, as can also be seen in Figure 8 (RIGHT). This hierarchy among the "Yukawa" coupling entries $|C_{ab}^{(9)}|$ means that on a logarithmic scale they are within a radius of $\Pi \sim 5.5$ (which means less than about 2-orders of 10-magnitude span in coupling values are needed). These results confirm that (4.14) naturally generates a neutrino mass matrix m_{ab}^{ν} with $m_{ee}^{\nu} \simeq 0$, where this is now understood as the mass matrix m_{ab}^{ν} from (4.14) with minimal degree of hierarchy in $C_{ab}^{(9)}$ while compatible with data from neutrino oscillation experiments. Notice that the minimal degree of hierarchy is slightly milder than the one present in the charged-lepton mass pattern

$$\min_N \sqrt{\left[\log\left(N m_{l_e}\right)\right]^2 + \left[\log\left(N m_{l_\mu}\right)\right]^2 + \left[\log\left(N m_{l_\tau}\right)\right]^2} \sim 6\,. \tag{4.16}$$

At this point, the dependence of the rest of neutrino mass matrix entries $|m_{ab}^{\nu}|$ with the amount of hierarchy Π becomes very important. In particular, this will favor one of the textures (3.4) with respect to the others in terms of hierarchy. In Figure 8 (LEFT) we show the size of the different entries $|m_{ab}^{\nu}|$ representing the minimal amount of hierarchy as a function of the lightest neutrino mass m. The element $|m_{ee}^{\nu}|$ is substantially smaller than $\left|m_{e\mu}^{\nu}\right|$ and both $|m_{ee}^{\nu}|$ and $\left|m_{e\mu}^{\nu}\right|$are much smaller than the other elements $|m_{ab}^{\nu}|$ (except for the region with large $m > 10^{-2}\,\text{eV}$ and Π, where $\left|m_{e\mu}^{\nu}\right|$ as the smallest element is favored). As shown in Figures 7 and 8 (RIGHT), the region with minimal hierarchy corresponds to $0.002\,\text{eV} < m < 0.007\,\text{eV}$ (the "chimney"), where $|m_{ee}^{\nu}| \simeq 2 \times 10^{-7}$ eV. From Figure 8 (LEFT) we see that $\left|m_{e\mu}^{\nu}\right|$ also decreases substantially within this region, and both $|m_{ee}^{\nu}|$ and $\left|m_{e\mu}^{\nu}\right|$ reach their minimal value ($|m_{ee}^{\nu}| \sim 10^{-7}$ eV, $\left|m_{e\mu}^{\nu}\right| \sim 10^{-5}$ eV) when the hierarchy is globally minimized, for $m \sim 0.0045$ eV. The fact that there is only one value of m for which both $|m_{ee}^{\nu}| \to 0$ and $\left|m_{e\mu}^{\nu}\right| \to 0$ can be easily understood by noticing that if $m_{ee}^{\nu} \simeq 0$ and $m_{e\mu}^{\nu} \simeq 0$, then fixing the oscillation parameters θ_{12}, θ_{13}, θ_{23}, Δm_{13}^2 and Δm_{21}^2 results in a unique prediction for δ, α_1, α_2 and m (recall the discussion from Section 3).

From the previous discussion, the texture with $m_{ee}^{\nu} \simeq 0$ and $m_{e\mu}^{\nu} \simeq 0$ emerges as the one that is most naturally generated from Eq. (4.14), as anticipated. However, as already stressed above, the possibility of realizing it (and the other textures in (3.4)) will also depend on the specific BSM completion to $\mathcal{O}^9$, since $C_{ab}^{(9)}/\Lambda$ cannot be arbitrarily small if one is to be compatible with neutrino oscillation data. In the next section we discuss the generic aspects of possible tree-level and loop-induced BSM completions to $\mathcal{O}^9$.

[9]Global minimization in multidimensional spaces is generically difficult. We found the `MATLAB` tool box with `GlobalSearch` setup and the `fmincon` option for finding minima of constrained nonlinear multivariable functions suited our task well.

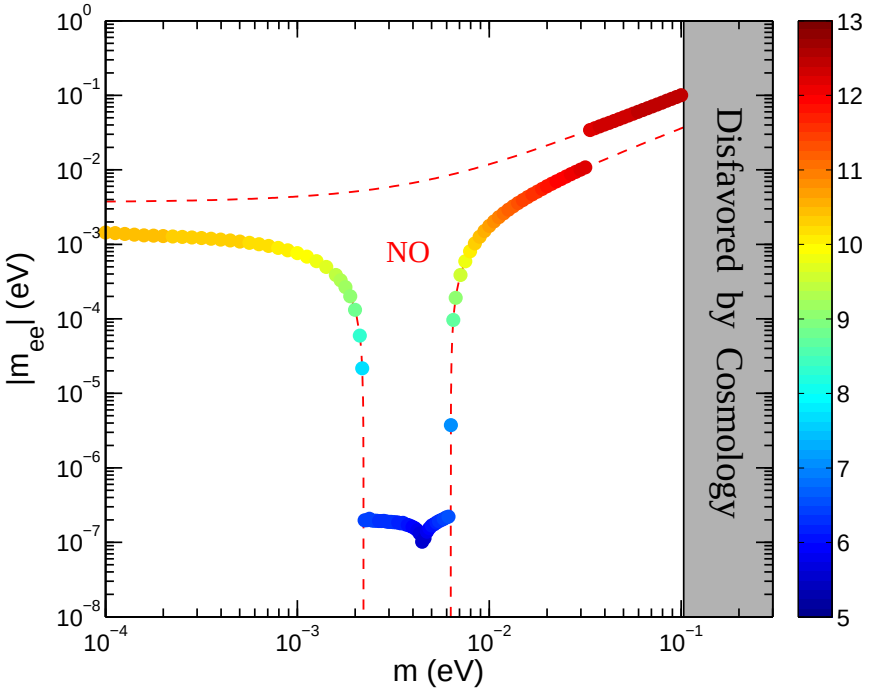

Figure 7: The minimal amount of Yukawa hierarchy Π (shown by the color-bar code on the right) as a function of the lightest neutrino mass m is shown in the $(m, |m^\nu_{ee}|)$ plane. A clear minimum in the hierarchy (dark blue) appears in a narrow range of m, where $|m^\nu_{ee}| \simeq 10^{-7}$ eV and $\Pi \simeq 5.5$. The region within the dashed-red lines corresponds to the allowed region for $|m^\nu_{ee}|$ in the case of normal ordering (NO) of neutrino masses. The parameters θ_{12}, θ_{13}, θ_{23}, Δm^2_{13} and Δm^2_{21} are fixed to their best-fit measured values [20].

4.2 Tree-level and loop-induced BSM completions of $\mathcal{O}^9$

We now explore the possible renormalizable completions[10] of $\mathcal{O}^9$ given in Eq. (4.12). The lepton bilinear $\overline{\ell^c}_{R_a}\,\ell_{R_b}$ is Lorentz and $SU(2)_L$ invariant, but has hypercharge $Y = -2$. The only possible completion[11] of $\overline{\ell^c}_{R_a}\,\ell_{R_b}$ then requires a scalar field ρ, $SU(2)_L$ singlet with hypercharge $Y = 2$, to form the renormalizable and $SU(2)_L \times U(1)_Y$ gauge invariant term $C_{ab}\,\overline{\ell^c}_{R_a}\,\ell_{R_b}\,\rho^{++}$, with C_{ab} a Yukawa matrix in flavor space. As the field ρ is a singlet under $SU(2)_L$, it does not couple directly to the W bosons. The extra field(s) needed to connect ρ^{++} to the W bosons will in turn determine whether the non-renormalizable operator $\mathcal{O}^9$ is induced at tree-level or at loop level.

For a tree-level completion, ρ^{++} has to mix with another state with nontrivial $SU(2)_L$ quantum numbers. The simplest possibility is then to introduce a scalar $SU(2)_L$ triplet field Δ with hypercharge $Y = 1$ [31, 32]

$$\Delta = \begin{pmatrix} \Delta^+/\sqrt{2} & \Delta^{++} \\ \Delta^0 & -\Delta^+/\sqrt{2} \end{pmatrix} \tag{4.17}$$

[10] A complete classification has been recently given in [72].

[11] As shown in [72], it is also possible to build renormalizable completions of $\mathcal{O}^9$ that do not involve the bilinear $\overline{\ell^c}_{R_a}\,\ell_{R_b}$ appearing explicitly in the Lagrangian. These completions however require a substantially larger amount of degrees of freedom, and we will not consider them in this work.

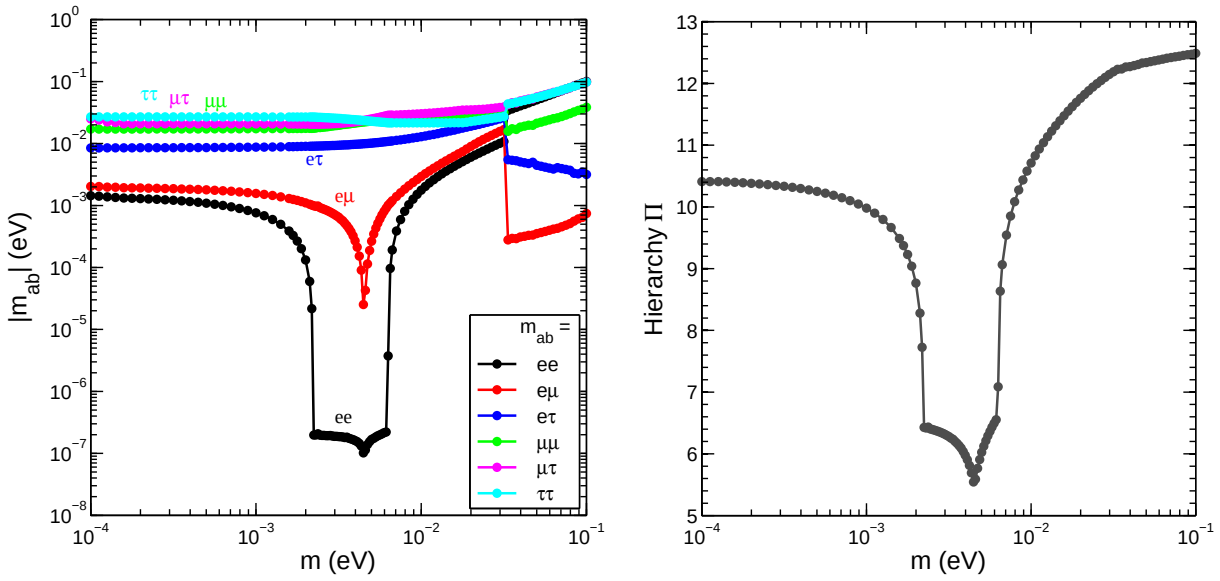

Figure 8: LEFT: Value of the different entries in the neutrino mass matrix $|m^{\nu}_{ab}|$ for the minimal hierarchy Π as a function of the lightest neutrino mass m (in the NO scenario). RIGHT: Value of the minimal hierarchy Π (defined in Eq. 4.15) as a function of m.

The Δ^{++} component of Δ may mix with ρ^{++} upon electroweak symmetry breaking, giving rise to two doubly charged mass eigenstates $\Delta^{++}_{1,2}$ with masses $m_{\Delta_{1,2}}$. At the same time, Δ^0 has to develop a *vev* upon electroweak symmetry breaking, since the coupling of $\Delta^{++}_{1,2}$ to W bosons is proportional to $\langle\Delta^0\rangle = v_\Delta$. In practice, two possible ways to obtain the Δ^{++}-ρ^{++} mixing (parametrized via a mixing angle θ_Δ) have been explored. The first is through an operator $H^\dagger\,\Delta\,\tilde{H}\,\rho$ (with H being the SM scalar doublet) [31, 51]. In this case θ_Δ may be sizable ($\sin(2\theta_\Delta) \sim v^2/m^2_{\Delta_{1,2}}$) if the masses $m_{\Delta_{1,2}}$ are close to the electroweak scale v. However, in this scenario the absence of a contribution to neutrino masses coming from a type-II see-saw mechanism cannot be consistently avoided (see discussion in [32]). A way to overcome this problem was proposed in [32], where the mixing is induced through an operator $\mathrm{Tr}\left[\Delta^\dagger\Delta^\dagger\right]\,\rho$. A (spontaneously broken) Z_2 symmetry is then used[12] to consistently avoid a type-II see-saw contribution to neutrino masses. However, the mixing angle θ_Δ is in this case suppressed ($\sin(2\theta_\Delta) \sim v_\Delta/m_{\Delta_{1,2}} \ll 1$) due to the smallness of the triplet *vev* needed to satisfy electroweak precision constraints ($v_\Delta \lesssim 5$ GeV $\ll v$).

An elegant solution to the above problems for tree-level completions is obtained through renormalizable completions at loop level. No mixing of the ρ field is necessary, but instead the ρ coupling to W bosons appears at 1-loop (or higher), which requires new fields charged under both $SU(2)_L$ and $U(1)_Y$. If the new fields respect a Z_2 symmetry, which remains unbroken after electroweak symmetry breaking, this guarantees that neutrino masses will first appear at 3 (or more) loops. Due to the Z_2 symmetry, these scenarios could automatically incorporate a stable dark matter candidate. A concrete realization of this idea is given in [34], which together with the ρ^{++} scalar field introduces two new fields which are odd

[12] As discussed in [32], the spontaneous breaking of this Z_2 symmetry, triggered by electroweak symmetry breaking, leads to a domain-wall problem in this scenario.

under the Z_2 symmetry discussed: an inert scalar $SU(2)_L$ doublet,

$$H_2 = \begin{pmatrix} \Lambda^+ \\ H_0 + i\, A_0 \end{pmatrix}, \tag{4.18}$$

and a scalar $SU(2)_L$ singlet, S^+, with hypercharge $Y = 1$. Altogether, the LNV part of the Lagrangian is given by

$$\begin{aligned} -\mathcal{L}_{LNV} = \;& C_{ab}\, \overline{\ell^c}_{R_a} \ell_{R_b}\, \rho^{++} + \tfrac{\lambda_5}{2} \left(H_1^\dagger H_2\right)^2 + \kappa_1\, H_2^T i\sigma_2 H_1\, S^- \\ & + \kappa_2\, \rho^{++} S^- S^- + \xi\, H_2^T i\sigma_2 H_1\, S^+\, \rho^{--} + \text{h.c.} \end{aligned} \tag{4.19}$$

Due to the κ_1-coupling in (4.19), the states S^+ and Λ^+ mix upon electroweak symmetry breaking (the mixing angle being θ^+), giving rise to two charged mass eigenstates $H^+_{1,2}$ with masses $m_{H^+_{1,2}}$. The states $H^+_{1,2}$, A_0 and H_0 thus have negative Z_2 parity (ρ^{++} has positive Z_2 parity), with the lightest state being either A_0 or H_0 in order to provide a viable dark matter candidate. In this model, the unbroken Z_2 symmetry results in the $\mathcal{O}^9$ operator being generated at 1-loop level, with neutrino masses appearing at 3-loops (see [34] for details). We want to stress that, as for the tree-level case, various (possibly many) loop realizations of the $\mathcal{O}^9$ operator may be possible.

A common feature of all the scenarios discussed above is the presence of the ρ^{++} scalar particle, coupling to right-handed charged leptons through a term $C_{ab}\, \overline{\ell^c}_{R_a}\, \ell_{R_b}\, \rho^{++}$. This scalar particle then mediates Lepton Flavor Violation (LFV) processes such as $\mu^+ \to e^+e^+e^-$, $\tau^- \to e^+e^-e^-$ or $\tau^- \to e^+\mu^-\mu^-$ at tree-level (the amplitude of each process $a \to b\,c\,d$ being proportional to $|C^*_{ab}C_{cd}|\,/m^2_\rho$) and $\mu^+ \to e^+\,\gamma$ at 1-loop. The experimental constraints on these processes are rather stringent, specially for the very rare decays $\mu^+ \to e^+e^+e^-$ and $\mu^+ \to e^+\,\gamma$, and the present scenarios predict their rates must be close to the current experimental limits [52, 53]. In addition, the LFV process $\tau^- \to e^+\mu^-\mu^-$ is also predicted close to the current experimental sensitivity, since the Yukawa couplings $C_{e\tau}$ and $C_{\mu\mu}$ cannot be very small in these scenarios in order to reproduce the correct values for the observed neutrino mass spectrum [32,34]. A detailed analysis of LFV constraints for these scenarios is however beyond the scope of this paper (see [54] for a study of LFV constraints on processes mediated by a ρ^{++} singlet scalar).

The discussion of this section highlights the feasibility of finding renormalizable completions of $\mathcal{O}^9$, both at tree-level and 1-loop level, and the main features of these completions. As discussed previously, the smallness of neutrino masses compared to the electroweak scale is naturally explained in these scenarios in terms of a 2 or 3-loop suppression, while the texture zeroes present in the neutrino mass matrix provide specific relations among the various neutrino oscillation parameters which satisfy the current experimental data and can be further tested in the near future. Furthermore, the $0\nu\beta\beta$ decay process in these models has rather unique features, which we will study in detail in the next section.

5 Neutrinoless double β-decay ($0\nu\beta\beta$)

Scenarios where LNV new physics couples directly only to right-handed charged leptons are very interesting for the potential $0\nu\beta\beta$ decay of atomic nuclei. As discussed in the previous

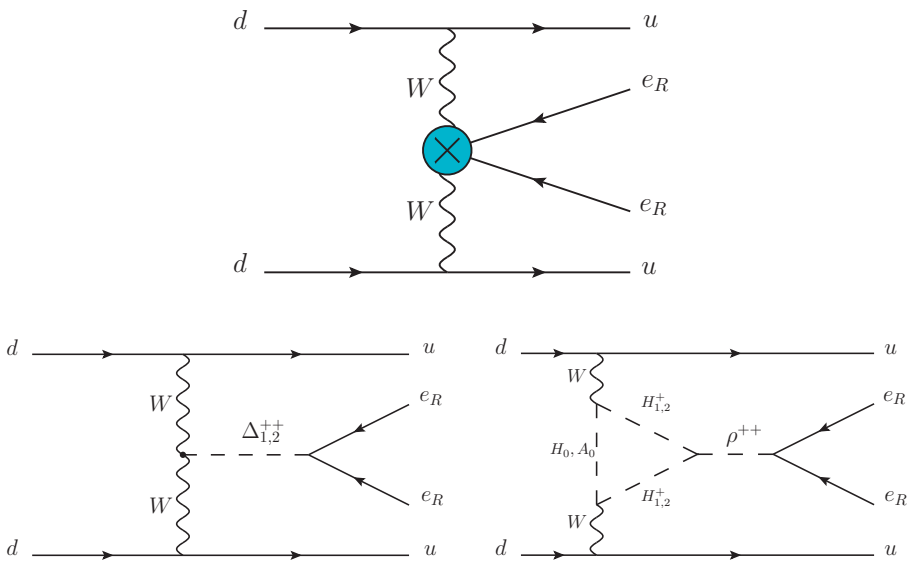

Figure 9: TOP: Effective $0\nu\beta\beta$ contribution from $\mathcal{O}^9$. BOTTOM-LEFT: $0\nu\beta\beta$ from tree-level BSM completions of $\mathcal{O}^9$. BOTTOM-RIGHT: $0\nu\beta\beta$ from 1-loop BSM completions of $\mathcal{O}^9$.

section, the operator $\mathcal{O}^9$ in Eq. (4.12) leads to a neutrino mass matrix m^ν_{ab} of the form (4.14) which then generically contains approximate zeroes $m^\nu_{ee} \simeq 0$, $m^\nu_{e\mu} \simeq 0$. As a result, the contribution from light neutrinos to the $0\nu\beta\beta$ decay amplitude, being proportional to $\mathcal{A}^\nu_{0\nu\beta\beta} \sim m^\nu_{ee}/\langle p^2\rangle$ with $\langle p^2\rangle \sim (100\,\text{MeV})^2$ the square of the typical momentum transfer between nucleons in the decay process [55], is extremely suppressed due to the smallness of m^ν_{ee}. Meanwhile, the contribution from the short-distance physics, encoded in the operator $\mathcal{O}^9$, contributes to the $0\nu\beta\beta$ decay (as shown in Figure 9) without suffering from the 2-loop and $m^2_{l_e}$ suppression that affects the light-neutrino exchange via the m^ν_{ee} factor (recall Figure 5 and (4.14)). This short-distance contribution would thus be the dominant source of $0\nu\beta\beta$ decays, and depending on the value of the C_{ee} (the Yukawa coupling from the renormalizable BSM theory, as discussed in Section 4.2), it could actually be large enough to make the process detectable in ongoing and future $0\nu\beta\beta$ decay experiments, including GERDA [37,38], EXO [39], SNO+ [40], KamLAND-Zen [41,42], CUORE [43], NEXT [44,45], MAJORANA [46] and SuperNEMO [47].

The effective 6-fermion contact interaction relevant for $0\nu\beta\beta$ decays, obtained from the short-distance contribution encoded in $\mathcal{O}^9$, can be written as (see [56, 57])

$$\mathcal{L}_{0\nu\beta\beta} = \frac{G_F^2}{2\,m_p}\,\epsilon_3\,J^\mu\,J_\mu\,\bar{e}(1-\gamma_5)e^c. \tag{5.20}$$

with the vector-axial (VA) hadronic currents being $J^\mu = \bar{u}\gamma^\mu(1-\gamma_5)d$. The parameter ϵ_3 encodes the information on the underlying BSM LNV physics, and may be written in terms of the Feynman amplitude $\mathcal{A}^{\text{SD}}_{0\nu\beta\beta}$ for the short-distance $0\nu\beta\beta$ process

$$\epsilon_3 = -2\,m_p\,\mathcal{A}^{\text{SD}}_{0\nu\beta\beta}\,. \tag{5.21}$$

The relevant, physically measurable quantity is the half-life $T^{0\nu\beta\beta}_{1/2}$ for various nuclei that can undergo $2\beta^-$ decay. In principle, contributions from all possible sources of $0\nu\beta\beta$ decay

have to be considered coherently. However, in scenarios where one source is dominant, the analysis simplifies considerably. Assuming respectively that the dominant contribution to the $0\nu\beta\beta$ process comes from the light-neutrino exchange or from the short-distance physics leading to (5.20), the half-life for the $0\nu\beta\beta$ process is very well approximated by either

$$\left[T_{1/2}^{0\nu\beta\beta}\right]^{-1} \simeq G_{01}\,\frac{|m_{ee}^{\nu}|^2}{m_{l_e}^2}\,|\mathcal{M}^{\nu}|^2 \qquad \text{or} \qquad \left[T_{1/2}^{0\nu\beta\beta}\right]^{-1} \simeq G_{01}\,|\epsilon_3|^2\,|\mathcal{M}^{\rm SD}|^2. \tag{5.22}$$

Here G_{01} is a phase-space factor characteristic for the specific decaying nucleus considered [58], and $\mathcal{M}^{\rm SD}$ (short-distance) and $\mathcal{M}^{\nu}$ (light-neutrino exchange) are the nuclear matrix elements (NME) that have to be calculated for each nucleus [56, 59, 60] (see also [55]). Equation (5.22) then allows to derive limits on m_{ee}^{ν} or ϵ_3 from the experimental bounds on the half-life of the $0\nu\beta\beta$ decay process.

As discussed above, in scenarios where $\mathcal{O}^9$ constitutes the leading source of LNV, the short-distance contribution to $0\nu\beta\beta$ decay largely dominates over the light-neutrino exchange one. As an illustration, we will now consider the tree-level [31, 32] and 1-loop [34] renormalizable completions to $\mathcal{O}^9$ discussed in section 4.2 (see Figure 9). For the tree-level case the $0\nu\beta\beta$ decay amplitude $\mathcal{A}_{0\nu\beta\beta}^{\rm SD}$ reads

$$\mathcal{A}_{0\nu\beta\beta}^{\rm tree} = \mathrm{s}_{2\theta_\Delta}\,v_\Delta\,\frac{\left(m_{\Delta_1}^2 - m_{\Delta_2}^2\right)}{m_{\Delta_1}^2\,m_{\Delta_2}^2}\,C_{ee}. \tag{5.23}$$

As expected, $\mathcal{A}_{0\nu\beta\beta}^{\rm tree}$ vanishes in the limit $m_{\Delta_1}^2 = m_{\Delta_2}^2$, since in this limit the $\Delta^{++} - \rho^{++}$ mixing term is absent from the Lagrangian and lepton number would be exactly conserved (recall the discussion in section 4.2). For the 1-loop case, the $0\nu\beta\beta$ decay amplitude $\mathcal{A}_{0\nu\beta\beta}^{\rm SD}$ can be computed in a straightforward way to give

$$\begin{aligned}\mathcal{A}_{0\nu\beta\beta}^{\rm loop} = \;& \tfrac{\Delta m_+^2\;\mathrm{s}_{2\theta^+}}{8\pi^2\;m_\rho^2}\,C_{ee}\;\times \\ & \Big\{\Big[\kappa_2\,\Delta m_+^2\,\mathrm{s}_{2\theta^+} - \xi\,v\,(\mathrm{c}_{\theta^+}^2\,m_{H_2^+}^2 + \mathrm{s}_{\theta^+}^2\,m_{H_1^+}^2)\Big]\,\Big[F_{H_1^+,H_2^+,H_0} - F_{H_1^+,H_2^+,A_0}\Big] \\ & -\xi\,v\,\Big[m_{H_0}^2\,F_{H_1^+,H_2^+,H_0} - m_{A_0}^2\,F_{H_1^+,H_2^+,A_0}\Big]\Big\}\end{aligned} \tag{5.24}$$

with $\Delta m_+^2 = m_{H_1^+}^2 - m_{H_2^+}^2$ and

$$F_{a,b,c} = \int_0^1 d\,x \int_0^{1-x} d\,y\,\frac{x\,y}{\left(x\,m_a^2 + y\,m_b^2 + (1-x-y)\,m_c^2\right)^2}\,. \tag{5.25}$$

It can then be verified using Eqs. (5.23) and (5.24) that both for the tree-level and 1-loop renormalizable completions, $\mathcal{A}_{0\nu\beta\beta}^{\rm SD} \gg \mathcal{A}_{0\nu\beta\beta}^{\nu}$.

Using the benchmark scenario from [32] ($m_{\Delta_1} = 10$ TeV, $m_{\Delta_2} = 2$ TeV, $v_\Delta = 2$ GeV and $\mathrm{s}_{2\theta_\Delta} = 0.00125$) and the benchmark scenario from [34] ($m_{H_0} = 70$ GeV, $m_{A_0} = 250$ GeV, $m_{H_1^+} = 90$ GeV, $m_{H_2^+} = 400$ GeV, $m_\rho = 1$ TeV, $\kappa_2 = 2$ TeV, $\xi = 0$ and $\mathrm{s}_{2\theta^+} = 1$), we respectively obtain for ϵ_3,

$$\epsilon_3^{\rm tree} = 1.13\times 10^{-9}\;|C_{ee}| \quad , \qquad \epsilon_3^{\rm loop} = 1.3\times 10^{-5}\;|C_{ee}|\;. \tag{5.26}$$

The predicted value for ϵ_3 may vary substantially depending on the specific tree-level/loop completion of $\mathcal{O}^9$, and the concrete values of the parameters within that scenario. However, (5.26) may be regarded as a rough guide of what is to be generically expected. The fact that $\epsilon_3^{\rm loop} \gg \epsilon_3^{\rm tree}$ in (5.26) can be understood noticing that the tree-level and 1-loop amplitudes roughly scale as $\mathcal{A}^{\rm tree}_{0\nu\beta\beta} \propto {\rm s}^2_{2\theta_\Delta}/m$ [32] and $\mathcal{A}^{\rm loop}_{0\nu\beta\beta} \propto 1/(4\pi)^2 \times {\rm s}^2_{2\theta^+}/m$ [34], respectively, with m being some $\mathcal{O}$(TeV) mass scale. The allowed value of the mixing angle in the tree-level case (${\rm s}_{2\theta_\Delta} \sim 0.001$) is much smaller than that of the 1-loop case (${\rm s}_{2\theta^+} \sim 1$), which results in $\mathcal{A}^{\rm loop}_{0\nu\beta\beta} \gg \mathcal{A}^{\rm tree}_{0\nu\beta\beta}$ despite the additional loop suppression factor $1/(4\pi)^2$.

We can compare the predictions in Eq. (5.26) with the current best experimental limits and future sensitivity prospects for five different nuclei that can undergo $2\beta^-$ decays: ^{76}Ge, ^{136}Xe, ^{150}Nd, ^{130}Te and ^{82}Se. In the following we detail the present and future experimental bounds on $T^{0\nu\beta\beta}_{1/2}$ for the different nuclei:

- ^{76}Ge: The recent results from the Phase I run of GERDA [38, 61] place the bound $T^{0\nu\beta\beta}_{1/2} > 2.1 \times 10^{25}\,$yr at 90 % C.L., while Phase II aims for a sensitivity of $T^{0\nu\beta\beta}_{1/2} > 2\times10^{26}\,$yr [37]. MAJORANA plans to have an ultimate sensitivity of $T^{0\nu\beta\beta}_{1/2} > 4\times10^{27}\,$yr [46] for the same nucleus after ~ 10 years of running.

- ^{136}Xe: The first results from the EXO-200 experiment set a bound $T^{0\nu\beta\beta}_{1/2} > 1.6\times10^{25}\,$yr at 90 % C.L. [62]. The sensitivity prospects for the EXO-1T upgrade is $T^{0\nu\beta\beta}_{1/2} > 8 \times 10^{26}\,$yr, and $T^{0\nu\beta\beta}_{1/2} > 1.3\times10^{28}\,$yr for the ultimate EXO-10T upgrade [63]. For the same nucleus, the current bound from the KamLAND-Zen experiment is $T^{0\nu\beta\beta}_{1/2} > 1.9\times10^{25}\,$yr at 90 % C.L. [42,64], with a future planned sensitivity of $T^{0\nu\beta\beta}_{1/2} > 4\times10^{26}\,$yr. The NEXT experiment aims to reach a sensitivity of $T^{0\nu\beta\beta}_{1/2} > 10^{26}\,$yr in the near future [45, 65].

- ^{150}Nd: The present bound from NEMO3 is $T^{0\nu\beta\beta}_{1/2} > 1.8\times10^{22}\,$yr at 90 % C.L. [66]. The NEMO3 upgrade, SuperNEMO, aims to reach a sensitivity of $T^{0\nu\beta\beta}_{1/2} > 5\times10^{25}\,$yr [47]. At the same time, the SNO+ experiment expects, after 4 years of data-taking, to reach a sensitivity of $T^{0\nu\beta\beta}_{1/2} > 1.6\times10^{25}\,$yr [67].

- ^{130}Te: The strongest bound for this nucleus is set by the CUORICINO experiment, $T^{0\nu\beta\beta}_{1/2} > 3\times10^{24}\,$yr at 90 % C.L. [68]. The CUORE experiment will substantially improve it, aiming for a sensitivity of $T^{0\nu\beta\beta}_{1/2} > 2\times10^{26}\,$yr in 5 years of data-taking [43].

- ^{82}Se: The strongest bound for this nucleus is currently set by NEMO3 with $T^{0\nu\beta\beta}_{1/2} > 3.6\times10^{23}\,$yr at 90 % C.L. [69, 70]. The planned sensitivity of SuperNEMO is $T^{0\nu\beta\beta}_{1/2} > 1.2\times10^{26}\,$yr [47].

In order to derive limits on ϵ_3 and m^ν_{ee}, we use the phase-space factors G_{01} computed in [58], and the NME values from [59] for light-neutrino exchange and from [60] for the short-distance contributions. The adopted values are given in Table 1. Note that different methods of evaluating NMEs can give different results by a factor $\sim 1.5-2$, which emergy from the specific approximations done in each method and their corresponding uncertainties

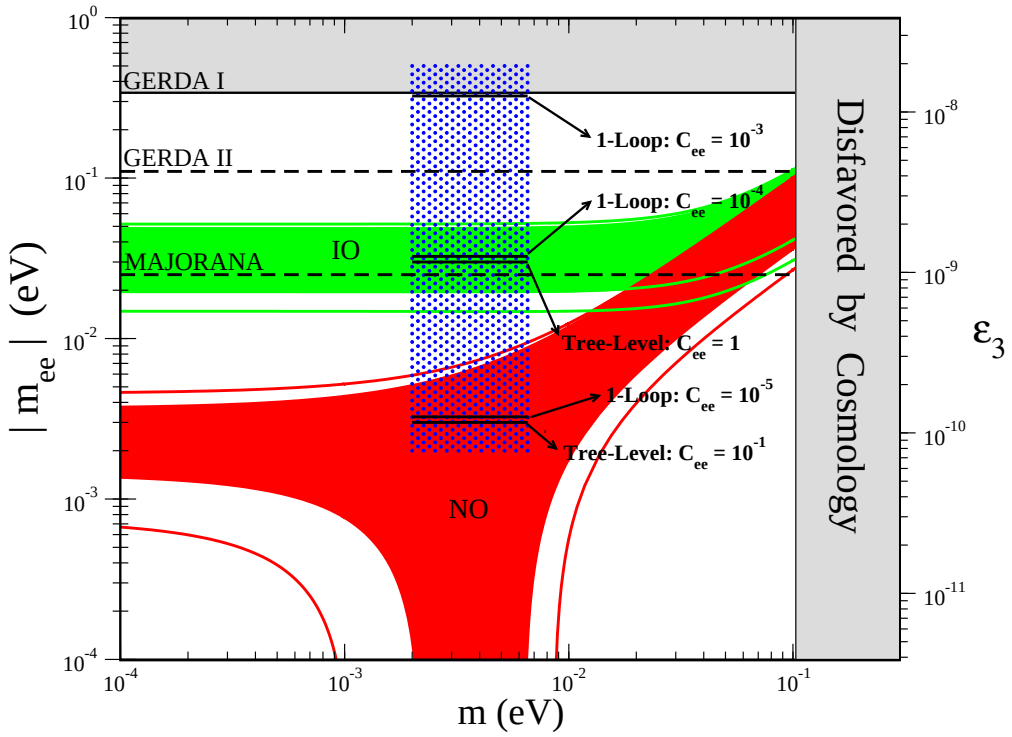

Figure 10: Current limits and future sensitivities on ϵ_3 and $|m^\nu_{ee}|$ from the ^{76}Ge experiments GERDA and MAJORANA (horizontal dashed-black lines), derived from $T^{0\nu\beta\beta}_{1/2}$ limits with $0\nu\beta\beta$ decay dominated by either short-distance physics (ϵ_3) or light-neutrino exchange ($|m^\nu_{ee}|$). Allowed $|m^\nu_{ee}|$ regions for normal ordering NO (red) and inverted ordering IO (green) are shown for neutrino oscillation parameters fixed to best-fit values (filled regions) and if allowed to vary within their 3σ uncertainty range (solid lines). The rectangle (dotted-blue) represents a generic region in the (m, ϵ_3) plane for scenarios featuring the short distance $\mathcal{O}^9$ operator in Eq. (4.12) (recall that these scenarios have NO with $|m^\nu_{ee}| \simeq 0$). Its enclosed horizontal solid-black lines are concrete Yukawa choices $C_{ee} = 10^{-3}, 10^{-4}, 10^{-5}$ (1-loop) and $C_{ee} = 1, 10^{-1}$ (tree-level) for the tree-level/1-loop renormalizable completion of $\mathcal{O}^9$ discussed in the text. The grey regions are currently excluded by cosmological observations and present $0\nu\beta\beta$ decay limits.

(see [59] for a more detailed discussion). This introduces some uncertainty to the derived limits on ϵ_3 and m^ν_{ee} that we quote here.

A comparison between current experimental limits and future expected sensitivities on $T^{0\nu\beta\beta}_{1/2}$ are presented as limits on ϵ_3 and m^ν_{ee} in Figures 10-12, for all the different nuclei discussed above. The predicted values of ϵ_3 for the tree-level and 1-loop completions of $\mathcal{O}^9$ (for different choices of $|C_{ee}|$), as well as the allowed region of m^ν_{ee} for NO and IO are also presented in these figures. It should be noted that the ratios $|m^\nu_{ee}|/\epsilon_3$ are different in these figures. This is due to the fact that for each nuclei the ratio $|\mathcal{M}^{\rm SD}|/|\mathcal{M}^\nu|$ is different (see Table 1). For ^{130}Te and ^{82}Se we find numerically very similar ratios $|\mathcal{M}^{\rm SD}|/|\mathcal{M}^\nu|$, and experiments involving these nuclei are therefore displayed together in Figure 12.

For the scenarios discussed in this work, with LNV induced by the effective operator $\mathcal{O}^9$, the short-distance contribution to $0\nu\beta\beta$ decays is by far dominant over long-range neutrino exchange (for $|C_{ee}| = 10^{-3}$ the value $|m^\nu_{ee}|$ is $\sim 10^{-8}$ eV for the 1-loop scenario in [34]

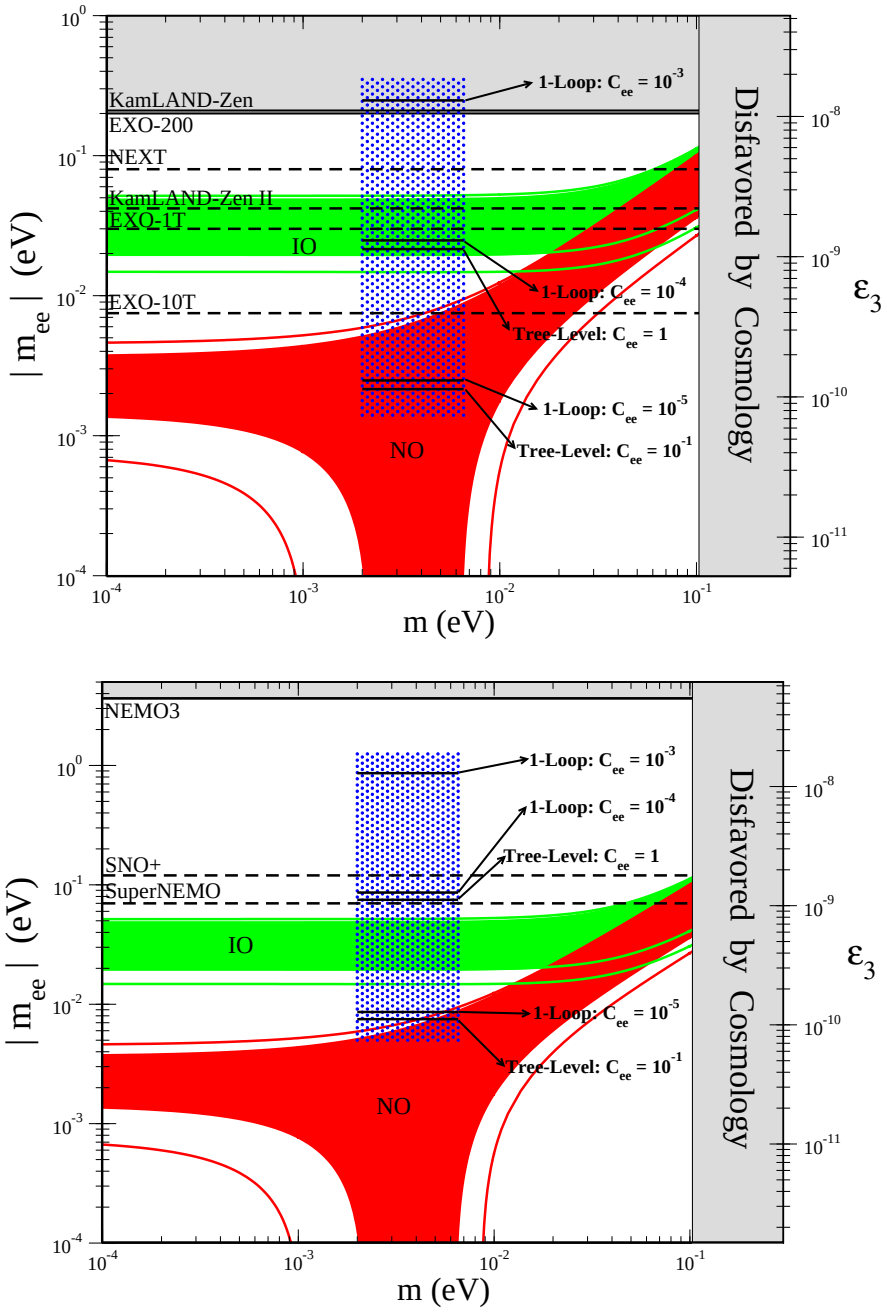

Figure 11: Same as Figure 10, for the ^{136}Xe experiments EXO, NEXT and KamLAND-Zen (TOP), and the ^{150}Nd experiments NEMO3, SNO+ and SuperNEMO (BOTTOM).

and does not even appear in the range covered by the figures 10-12). It is seen that for not too small value of $|C_{ee}|$ the short-distance contribution to $0\nu\beta\beta$ decays could be within reach by both current and future experiments, in particular for 1-loop completions of $\mathcal{O}^9$ (for the specific 1-loop scenario presented here, the current limits on $T_{1/2}^{0\nu\beta\beta}$ already constrain $|C_{ee}|$ to be smaller than about 10^{-3}). At the same time, a detection of $0\nu\beta\beta$ decay in an ongoing or a future experiments, combined with an independent measurement excluding the IO for neutrino masses from neutrino oscillation experiments, would suggest a short-

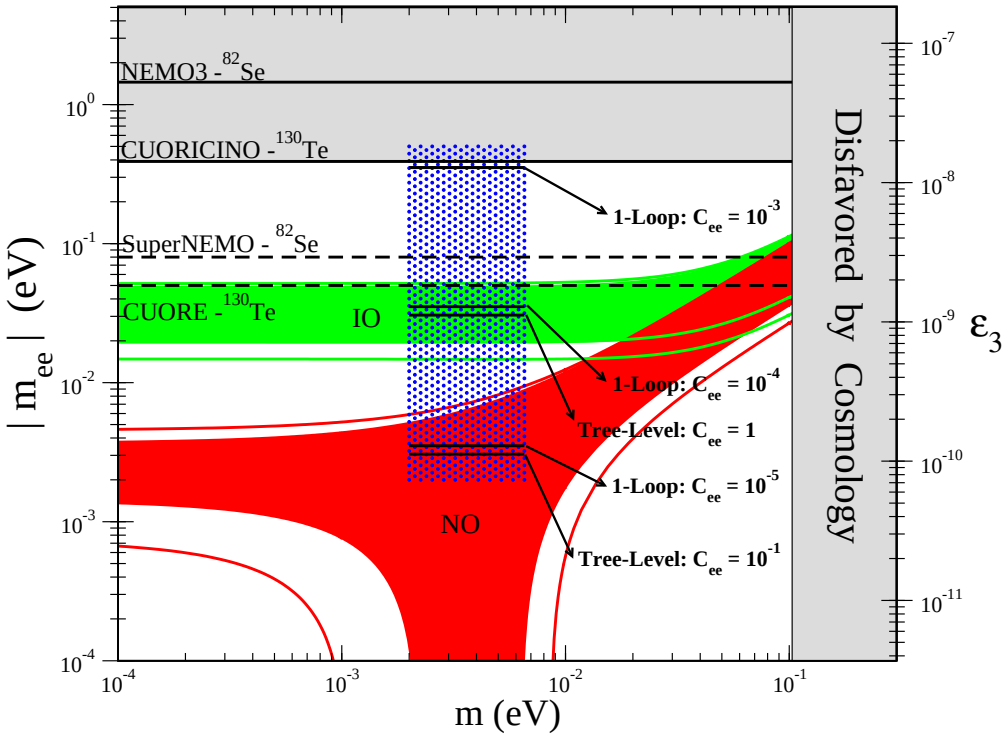

Figure 12: Same as Figure 10, for the ^{130}Te experiments CUORICINO and CUORE, and the ^{82}Se experiments NEMO3 and SuperNEMO. Note that ^{130}Te and ^{82}Se can be presented in the same plot as their $|\mathcal{M}^{\rm SD}|/|\mathcal{M}^{\nu}|$ ratios are numerically very similar (see text and Table 1).

	G_{01} $(10^{-14}\,\mathrm{yr}^{-1})$	$\lvert\mathcal{M}^{\nu}\rvert$	$\lvert\mathcal{M}^{\rm SD}\rvert$
^{76}Ge	0.623	4.07	213
^{136}Xe	4.31	2.82	109
^{150}Nd	19.2	2.33	311
^{130}Te	4.09	3.63	198
^{82}Se	2.70	3.48	192

Table 1: Values used for the phase-space factors G_{01} for the different nuclei, taken from [58]. The nuclear matrix elements (NMEs) $|\mathcal{M}^{\nu}|$ are the averaged best-estimates from [59]. The NMEs $\left|\mathcal{M}^{\rm SD}\right|$ are the values given in [60] from their computation using the pn-QRPA approach.

distance physics origin for the $0\nu\beta\beta$ decay signal. Very large $0\nu\beta\beta$ signal would also not be possible from light-neutrino exchange, as it requires a degenerate neutrino mass spectrum with $m > 0.1$ eV, which is clearly disfavoured by present cosmological data.

Another consequence of the operator $\mathcal{O}^9$ leading to $0\nu\beta\beta$ decays is that the two emitted electrons would be right-handed (as opposed to the usual contribution from light-neutrino exchange, where the two emitted electrons are left-handed). A (hypothetical) measurement of the chirality of the emitted electrons would allow to further test $\mathcal{O}^9$ as responsible for LNV and generation of Majorana neutrino masses.

6 Conclusions

Links between the origin of neutrino masses, the observed structure of neutrino masses and mixings, and $0\nu\beta\beta$ decay probes of the Majorana nature of neutrinos may provide a key to a unified understanding of these various central aspects of Neutrino Physics. Potentially, all these concepts are linked and generated by the same underlying new physics. We have explored a simple class of theories beyond the SM that explain the large existing hierarchy between the scale of neutrino masses and the electroweak scale by radiatively induced neutrino masses (exemplified by explicit known 2-loop and 3-loop scenarios) and that connect to specific neutrino mixing properties due to approximate zeroes in the neutrino mass matrix m^{ν}_{ab}. In these theories, new physics beyond the SM responsible for LNV and the generation of Majorana neutrino masses does not couple directly to quarks or left-handed leptons, but couples to right-handed leptons. The consequence is that the leading (and dominant) contributions to lepton number violation (LNV) and neutrino masses are encoded in a single non-renormalizable dimension nine operator, $\mathcal{O}^9$ in Eq. (4.12).

The present analysis shows the way approximate texture zeroes $m^{\nu}_{ee} \simeq 0$ and $m^{\nu}_{e\mu} \simeq 0$ naturally emerge in this class of theories. We have also defined a measure of the amount of hierarchy needed in the underlying Yukawa matrix generating the neutrino mass matrix. Once $m^{\nu}_{ee} \simeq 0$ and $m^{\nu}_{e\mu} \simeq 0$ the rest of the entries of m^{ν}_{ab} are required to be of the same size in order to be compatible with current neutrino oscillation data, which then requires a mild amount of hierarchy in the Yukawa couplings (although less than the one present in the charged-lepton sector of the SM).

The texture with zeroes $m^{\nu}_{ee} \simeq 0$ and $m^{\nu}_{e\mu} \simeq 0$ generated in this class of theories gives rise to nontrivial correlations among the different neutrino parameters. These correlations can accommodate the current data from neutrino oscillation experiments while giving testable predictions for the unknowns in the neutrino sector, such as a normal neutrino mass ordering (NO) and a strong correlation among the values of the reactor angle θ_{13}, the atmospheric angle θ_{23} (and its octant) and the CP phase δ (see Figures 1-4 for various correlations). We also show that future, more precise measurements of $|\Delta m^2_{31}|$ and the value of the solar angle θ_{12} will be crucial for an ultimate test of this correlation.

Finally, this class of theories also incorporate an important link to $0\nu\beta\beta$ decay, since a generic feature of these scenarios is the existence of a contribution to $0\nu\beta\beta$ decay from short-distance physics which largely dominates over the one coming from light-neutrino exchange (extremely suppressed in these scenarios, since $m^{\nu}_{ee} \simeq 0$) and can be sizable in many cases. We have analyzed the features of this leading, short-distance contribution to $0\nu\beta\beta$ decay in concrete scenarios and derived prospects of detection in both ongoing and upcoming $0\nu\beta\beta$ decay experiments such as GERDA, EXO, SNO+, KamLAND-Zen, CUORE, NEXT, MAJORANA and SuperNEMO. Remarkably, these scenarios may provide a detectable signal in $0\nu\beta\beta$ decay together with a normal ordering (NO) for neutrino masses and a lightest neutrino mass $m \lesssim 0.01$ eV. A future combination of data from neutrino oscillation experiments, cosmology and $0\nu\beta\beta$ decay could allow to ultimately test $\mathcal{O}^9$ as responsible for lepton number vialotaion and the generation of neutrino masses.

Acknowledgements

We thank M. Maltoni and T. Schwetz for sharing with us data from their global fits [20]. M.G. thanks T. Schwetz for useful discussions and comments. J.M.N. thanks S. Pascoli for useful discussions, and A. Merle for discussions and useful comments on the manuscript. M.G. is supported by the Belgian Science Policy (IAP VI/11), the IISN and the ARC project 'Beyond Einstein: fundamental aspects of gravitational interactions'. J.M.N. is supported by the Science Technology and Facilities Council (STFC) under grant No. ST/J000477/1. M.R. is supported by Fondecyt grant No. 11110472, Anillo "Atlas Andino" ACT1102 and DGIP grant No. 11.12.39.

Appendix A. Master formula for $m_{ee} = m_{e\mu} = 0$

Equation (2.5) and (2.6), for the texture $m_{ee} = m_{e\mu} = 0$, can be rewritten as

$$\frac{m_1}{m_3} = e^{2i\alpha_i}\frac{s_{13}}{c_{13}^2}\left(s_{13} - t_{12}t_{23}e^{i\delta}\right) \equiv A \tag{A.1}$$

$$\frac{m_2}{m_3} = e^{2i(\alpha_2-\alpha_i)}\frac{s_{13}}{c_{13}^2}\left(s_{13} + t_{12}^{-1}t_{23}e^{i\delta}\right) \equiv B. \tag{A.2}$$

Equations (A.1) and (A.2) can then be express as

$$|m_1|^2 = \frac{\Delta m_{31}^2|A|^2}{1-|A|^2} \text{ or } |m_3|^2 = \frac{\Delta m_{31}^2}{1-|A|^2}, \tag{A.3}$$

$$\cos\delta = -\frac{t_{23}^2(1-t_{12}^4) + t_{12}^2(1+t_{23}^2t_{12}^2 - t_{13}^{-2})\frac{\Delta m_{21}^2}{\Delta m_{31}^2}}{2s_{13}t_{12}t_{23}(1+t_{12}^2 - t_{12}^2\frac{\Delta m_{21}^2}{\Delta m_{31}^2})} \tag{A.4}$$

where

$$|A|^2 = \frac{s_{13}^2(s_{13}^2 + t_{12}^2t_{23}^2 - 2s_{13}t_{12}t_{23}\cos\delta)}{c_{13}^4} \tag{A.5}$$

A convenient rewriting of Eq. (A.4) then gives (3.9). If Eq. (A.3) and (A.4) are fulfilled, then Eq. (A.1) and (A.2) can always be satisfied with proper chosen values of $\alpha_{1,2}$:

$$\tan 2\alpha_1 = \frac{-\sin\delta}{\cos\delta - s_{13}t_{12}^{-1}t_{23}^{-1}} \tag{A.6}$$

$$\tan 2(\alpha_2-\alpha_1) = \frac{-\sin\delta}{\cos\delta + s_{13}t_{12}t_{23}^{-1}} \tag{A.7}$$

Since α_1 and $\alpha_1+\alpha_2$ are still free up to a multiple of $\pi/2$, this allows to also choose the sign of A and B. The allowed region of neutrino parameters can now comprehensively be expressed as

$$|\cos\delta| \leq 1 \quad \text{with} \quad \begin{cases} |A| < 1 \;\Leftrightarrow\; \text{(NO)} \\ |A| > 1 \;\Leftrightarrow\; \text{(IO)} \end{cases} \tag{A.8}$$

An illustration of the correlation regions from Eq. (A.8) is shown as a slice in the neutrino mixing parameter space in Figure 13.

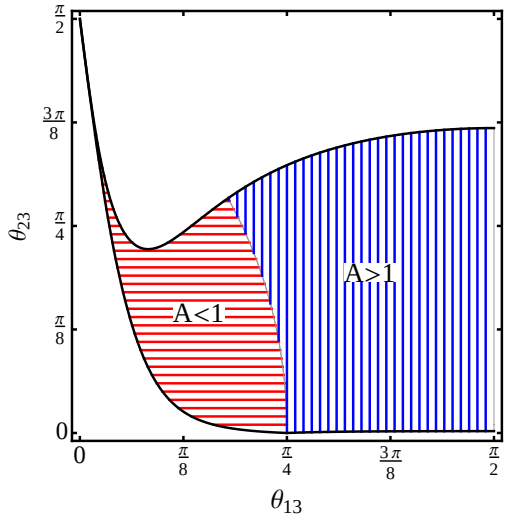

Figure 13: Allowed region $|\cos\delta| \leq 1$ in the $(\theta_{13}, \theta_{23})$ plane with Δm^2_{31}, Δm^2_{21} and s^2_{12} set to their best-fit values [20]. Normal ordering ($|A| < 1$) and inverted ordering (($|A| > 1$)) are indicated in the plot. Derived under the constraint $m_{ee} = m_{e\mu} = 0$.

References

[1] R. N. Mohapatra, S. Antusch, K. S. Babu, G. Barenboim, M. -C. Chen, A. de Gouvea, P. de Holanda and B. Dutta *et al.*, Rept. Prog. Phys. **70** (2007) 1757 [hep-ph/0510213].

[2] A. Zee, Phys. Lett. B **93** (1980) 389 [Erratum-ibid. B **95** (1980) 461]; Nucl. Phys. B **264** (1986) 99.

[3] K. S. Babu, Phys. Lett. B **203** (1988) 132.

[4] L. M. Krauss, S. Nasri and M. Trodden, Phys. Rev. D **67** (2003) 085002 [hep-ph/0210389].

[5] E. Ma, Phys. Rev. D **73** (2006) 077301 [hep-ph/0601225].

[6] M. Aoki, S. Kanemura and O. Seto, Phys. Rev. Lett. **102** (2009) 051805 [arXiv:0807.0361 [hep-ph]].

[7] S. Morisi and J. W. F. Valle, Fortsch. Phys. **61** (2013) 466 [arXiv:1206.6678 [hep-ph]].

[8] L. J. Hall, H. Murayama and N. Weiner, Phys. Rev. Lett. **84** (2000) 2572 [hep-ph/9911341].

[9] B. Pontecorvo, Sov. Phys. JETP **7** (1958) 172 [Zh. Eksp. Teor. Fiz. **34** (1957) 247]; Z. Maki, M. Nakagawa and S. Sakata, Prog. Theor. Phys. **28** (1962) 870.

[10] P. F. Harrison, D. H. Perkins and W. G. Scott, Phys. Lett. B **530** (2002) 167.

[11] F. P. An *et al.* [DAYA-BAY Collaboration], Phys. Rev. Lett. **108** (2012) 171803.

[12] J. K. Ahn *et al.* [RENO Collaboration], Phys. Rev. Lett. **108** (2012) 191802.

[13] Y. Abe *et al.* [DOUBLE-CHOOZ Collaboration], Phys. Rev. Lett. **108** (2012) 131801; Y. Abe *et al.* [DOUBLE-CHOOZ Collaboration], Phys. Rev. D **86** (2012) 052008.

[14] K. Abe *et al.* [T2K Collaboration], Phys. Rev. Lett. **107** (2011) 041801.

[15] P. Adamson *et al.* [MINOS Collaboration], Phys. Rev. Lett. **107** (2011) 181802; P. Adamson *et al.* [MINOS Collaboration], Phys. Rev. Lett. **108** (2012) 191801.

[16] R. Wendell *et al.* [Super-Kamiokande Collaboration], Phys. Rev. D **81** (2010) 092004 [arXiv:1002.3471 [hep-ex]].

[17] Y. Itow, Nucl. Phys. Proc. Suppl. **235-236** (2013) 79.

[18] D. V. Forero, M. Tortola and J. W. F. Valle, Phys. Rev. D **86** (2012) 073012

[19] G. L. Fogli, E. Lisi, A. Marrone, D. Montanino, A. Palazzo and A. M. Rotunno, Phys. Rev. D **86** (2012) 013012.

[20] M. C. Gonzalez-Garcia, M. Maltoni, J. Salvado and T. Schwetz, JHEP **1212** (2012) 123.

[21] P. H. Frampton, S. L. Glashow and D. Marfatia, Phys. Lett. B **536** (2002) 79.

[22] W. -l. Guo and Z. -z. Xing, Phys. Rev. D **67** (2003) 053002.

[23] A. Merle and W. Rodejohann, Phys. Rev. D **73** (2006) 073012.

[24] S. Dev, S. Kumar, S. Verma and S. Gupta, Phys. Rev. D **76** (2007) 013002.

[25] H. Fritzsch, Z. -z. Xing and S. Zhou, JHEP **1109** (2011) 083.

[26] P. O. Ludl, S. Morisi and E. Peinado, Nucl. Phys. B **857** (2012) 411.

[27] W. Grimus and P. O. Ludl, J. Phys. G **40** (2013) 055003.

[28] W. Grimus and P. O. Ludl, JHEP **1212** (2012) 117.

[29] S. Pascoli, S. T. Petcov and L. Wolfenstein, Phys. Lett. B **524** (2002) 319; Z. -z. Xing, Phys. Rev. D **68** (2003) 053002; S. Choubey and W. Rodejohann, Phys. Rev. D **72** (2005) 033016; M. Lindner, A. Merle and W. Rodejohann, Phys. Rev. D **73** (2006) 053005.

[30] P. A. R. Ade *et al.* [Planck Collaboration], arXiv:1303.5076 [astro-ph.CO].

[31] C. -S. Chen, C. Q. Geng and J. N. Ng, Phys. Rev. D **75** (2007) 053004.

[32] F. del Aguila, A. Aparici, S. Bhattacharya, A. Santamaria and J. Wudka, JHEP **1205** (2012) 133.

[33] F. del Aguila, A. Aparici, S. Bhattacharya, A. Santamaria and J. Wudka, JHEP **1206** (2012) 146.

[34] M. Gustafsson, J. M. No and M. A. Rivera, Phys. Rev. Lett. **110** (2013) 211802.

[35] Y. Farzan, S. Pascoli and M. A. Schmidt, JHEP **1303** (2013) 107.

[36] S. Weinberg, Phys. Rev. Lett. **43** (1979) 1566.

[37] S. .Schonert *et al.* [GERDA Collaboration], Nucl. Phys. Proc. Suppl. **145** (2005) 242.

[38] M. Agostini, M. Allardt, E. Andreotti, A. M. Bakalyarov, M. Balata, I. Barabanov, M. B. Heider and N. Barros *et al.*, arXiv:1307.4720 [nucl-ex].

[39] D. Akimov, G. Bower, M. Breidenbach, R. Conley, E. Conti, M. Danilov, R. DeVoe and Z. Djurcic *et al.*, Nucl. Phys. Proc. Suppl. **138** (2005) 224.

[40] M. C. Chen, Nucl. Phys. Proc. Suppl. **145** (2005) 65.

[41] T. Mitsui [KamLAND Collaboration], Nucl. Phys. Proc. Suppl. **217** (2011) 89.

[42] A. Gando *et al.* [KamLAND-Zen Collaboration], Phys. Rev. C **85** (2012) 045504.

[43] C. Arnaboldi *et al.* [CUORE Collaboration], Nucl. Instrum. Meth. A **518** (2004) 775; R. Ardito, C. Arnaboldi, D. R. Artusa, F. T. Avignone, III, M. Balata, I. Bandac, M. Barucci and J. W. Beeman *et al.*, hep-ex/0501010.

[44] F. Granena *et al.* [NEXT Collaboration], arXiv:0907.4054 [hep-ex].

[45] J. J. Gomez-Cadenas, J. Martin-Albo and F. Monrabal, JINST **7** (2012) C11007 [arXiv:1210.0341 [physics.ins-det]].

[46] R. Gaitskell *et al.* [Majorana Collaboration], nucl-ex/0311013.

[47] R. Arnold *et al.* [SuperNEMO Collaboration], Eur. Phys. J. C **70** (2010) 927 [arXiv:1005.1241 [hep-ex]].

[48] K. S. Babu and C. N. Leung, Nucl. Phys. B **619** (2001) 667.

[49] A. de Gouvea and J. Jenkins, Phys. Rev. D **77** (2008) 013008.

[50] P. W. Angel, N. L. Rodd and R. R. Volkas, arXiv:1212.6111 [hep-ph].

[51] C. -S. Chen, C. -Q. Geng, J. N. Ng and J. M. S. Wu, JHEP **0708** (2007) 022.

[52] U. Bellgardt *et al.* [SINDRUM Collaboration], Nucl. Phys. B **299** (1988) 1.

[53] J. Adam *et al.* [MEG Collaboration], Phys. Rev. Lett. **110** (2013) 201801 [arXiv:1303.0754 [hep-ex]].

[54] M. Nebot, J. F. Oliver, D. Palao and A. Santamaria, Phys. Rev. D **77** (2008) 093013 [arXiv:0711.0483 [hep-ph]].

[55] M. Blennow, E. Fernandez-Martinez, J. Lopez-Pavon and J. Menendez, JHEP **1007** (2010) 096.

[56] H. Pas, M. Hirsch, H. V. Klapdor-Kleingrothaus and S. G. Kovalenko, Phys. Lett. B **498** (2001) 35 [hep-ph/0008182].

[57] J. Bergstrom, A. Merle and T. Ohlsson, JHEP **1105** (2011) 122 [arXiv:1103.3015 [hep-ph]].

[58] J. Suhonen and O. Civitarese, Phys. Rept. **300** (1998) 123.

[59] J. J. Gomez-Cadenas, J. Martin-Albo, M. Sorel, P. Ferrario, F. Monrabal, J. Munoz-Vidal, P. Novella and A. Poves, JCAP **1106** (2011) 007 [arXiv:1010.5112 [hep-ex]].

[60] F. F. Deppisch, M. Hirsch and H. Pas, J. Phys. G **39** (2012) 124007 [arXiv:1208.0727 [hep-ph]].

[61] C. Macolino, arXiv:1312.0562 [hep-ex].

[62] M. Auger *et al.* [EXO Collaboration], Phys. Rev. Lett. **109** (2012) 032505 [arXiv:1205.5608 [hep-ex]].

[63] K. Wamba [EXO Collaboration], SLAC-WP-068.

[64] A. Gando *et al.* [KamLAND-Zen Collaboration], Phys. Rev. Lett. **110** (2013) 6, 062502 [arXiv:1211.3863 [hep-ex]].

[65] J. J. Gomez-Cadenas, J. Martin-Albo, M. Mezzetto, F. Monrabal and M. Sorel, Riv. Nuovo Cim. **35** (2012) 29 [arXiv:1109.5515 [hep-ex]].

[66] J. Argyriades *et al.* [NEMO Collaboration], Phys. Rev. C **80** (2009) 032501 [arXiv:0810.0248 [hep-ex]].

[67] J. Maneira [SNO+ Collaboration], J. Phys. Conf. Ser. **447** (2013) 012065.

[68] C. Arnaboldi *et al.* [CUORICINO Collaboration], Phys. Rev. C **78** (2008) 035502 [arXiv:0802.3439 [hep-ex]].

[69] R. Arnold *et al.* [NEMO Collaboration], Phys. Rev. Lett. **95** (2005) 182302 [hep-ex/0507083].

[70] A. S. Barabash *et al.* [NEMO Collaboration], Phys. Atom. Nucl. **74** (2011) 312 [arXiv:1002.2862 [nucl-ex]].

[71] http://www.nu-fit.org/?q=node/8

[72] A. Aparici, arXiv:1312.0554 [hep-ph].